Scientific Report No. 57

INVESTIGATION OF ELECTROMAGNETIC FIELDS IN MINE ENVIRONMENTS

by

James R. Wait
David A. Hill
David C. Chang

May 1980

Electromagnetics Laboratory
Department of Electrical Engineering
University of Colorado
Boulder, Colorado 80309

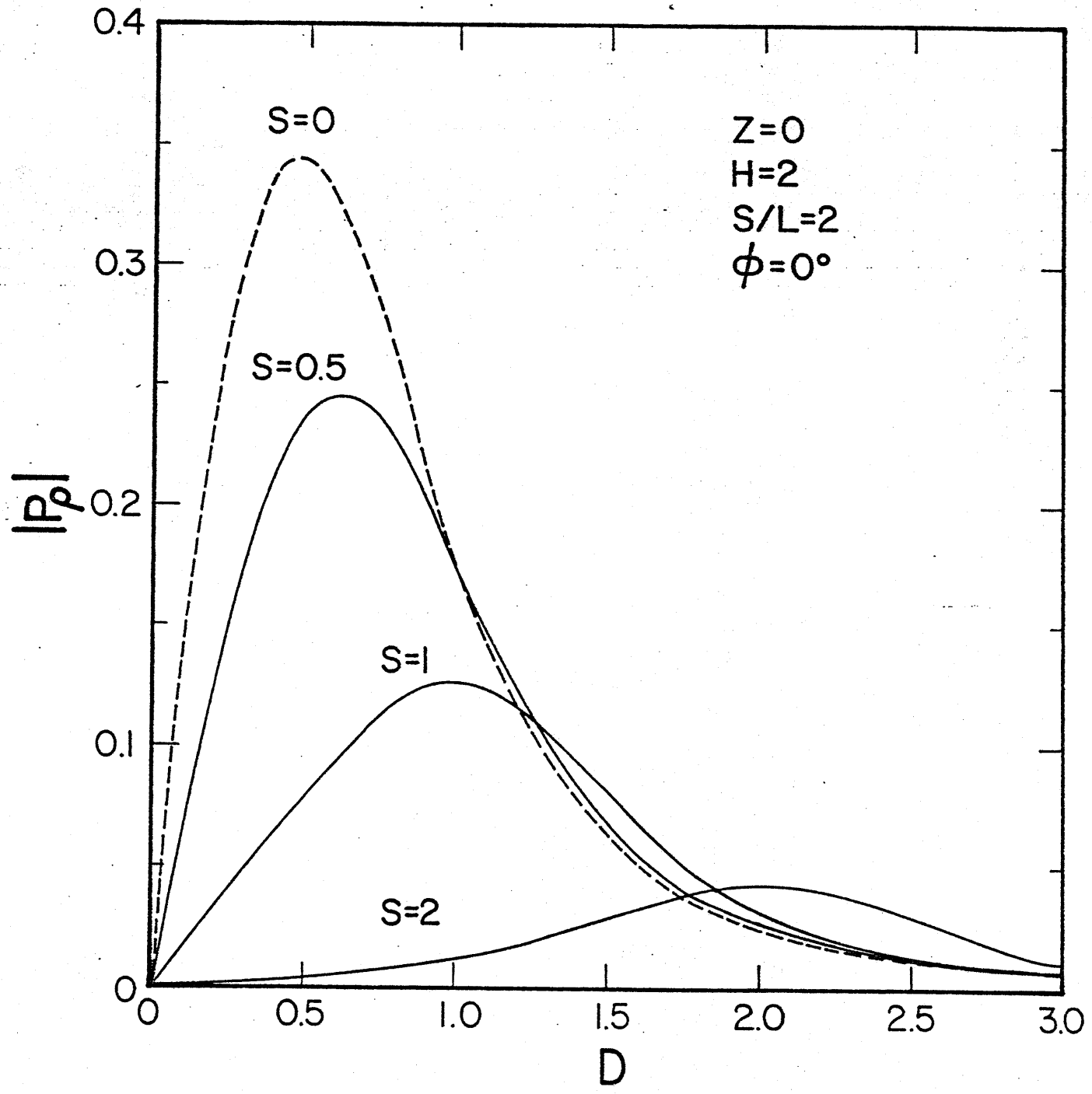

Radial component of normalized magnetic field for a rectangular loop for H = 5. Fig. 10

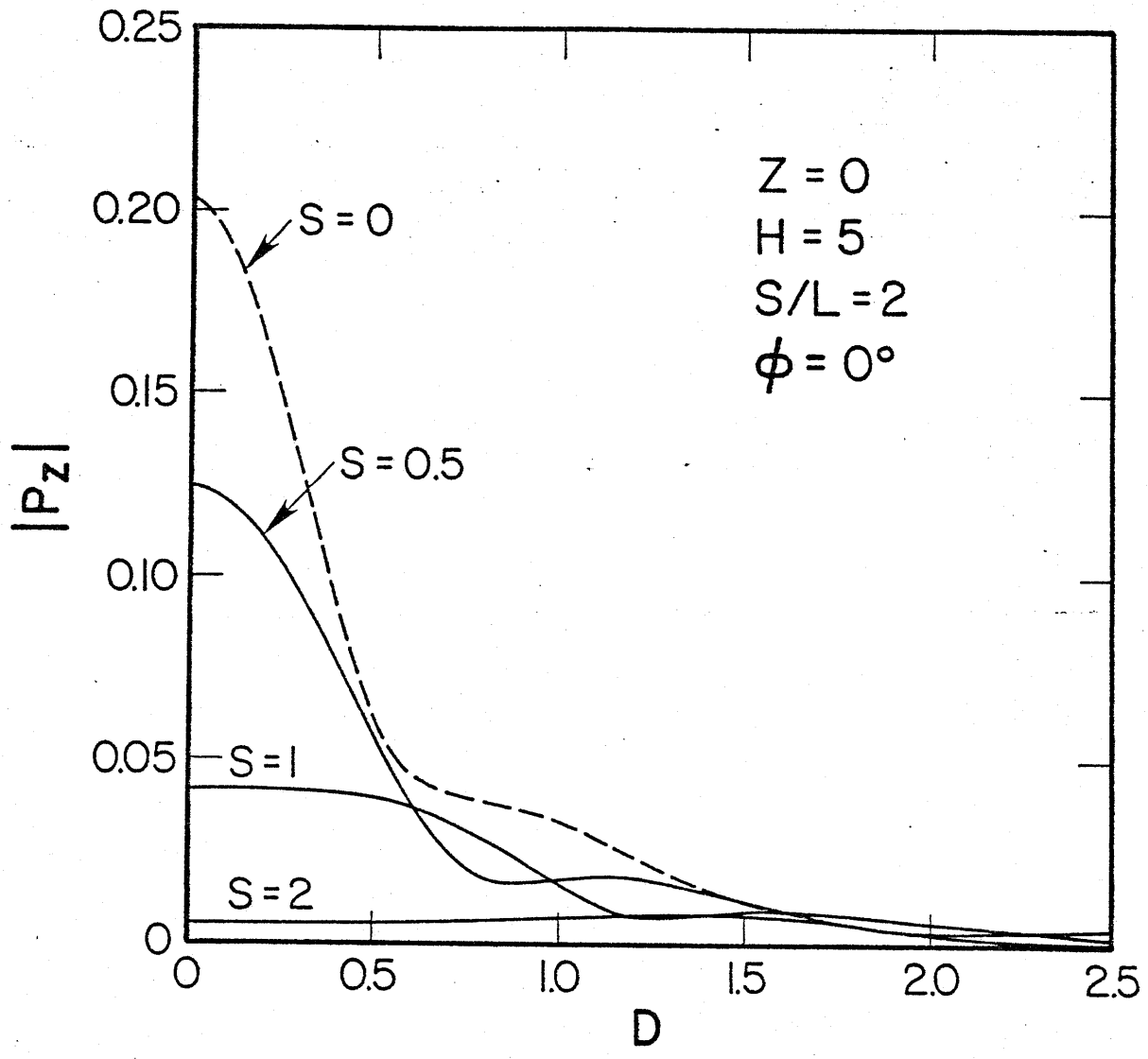

Vertical component of normalized magnetic field for a rectangular loop for H = 5. Fig. 11

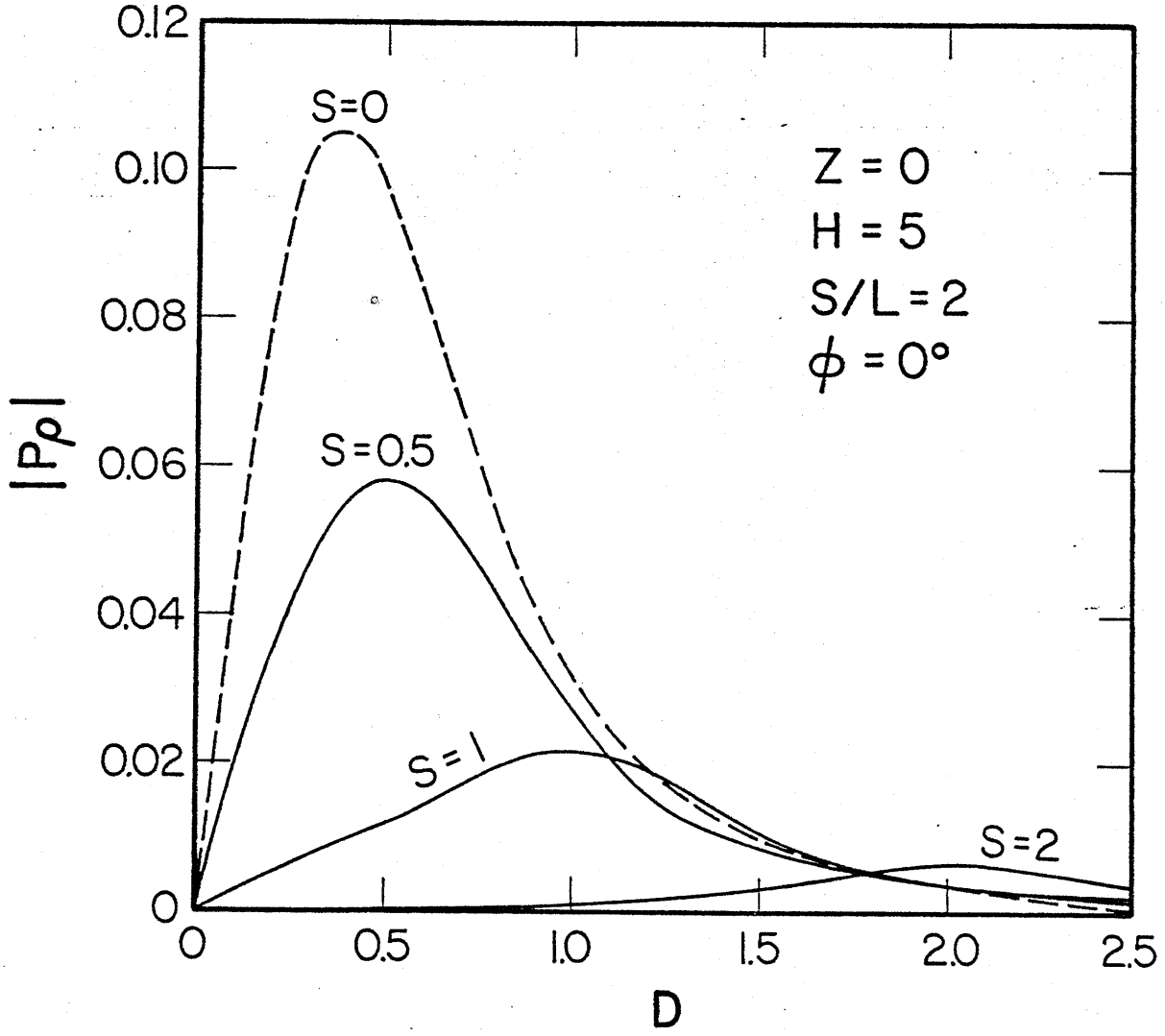

Radial component of normalized magnetic field for a rectangular loop for H = 5.

Fig. 12

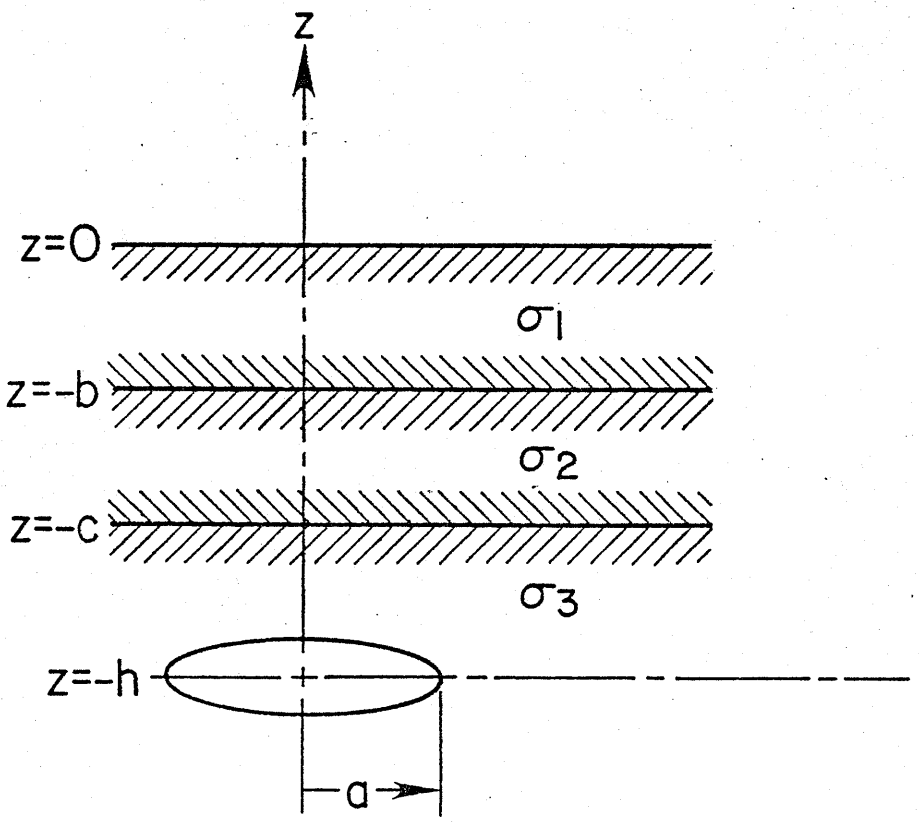

Magnetic dipole buried in three layer earth

Fig. 13

REPORT DOCUMENTATION PAGE

1. Report No.	2.	3. Recipient's Accession No.

4. Title and Subtitle

INVESTIGATION OF ELECTROMAGNETIC FIELDS IN MINE ENVIRONMENTS

5. Report Date
15 May 1980

6.

7. Author(s) James R. Wait (Members of Electromagnetics
David A. Hill Laboratory, University of Colo.)
David C. Chang

8. Performing Organization Report No.

9. Performing Organization Name and Address
Institute for Telecommunication Sciences
U.S. Dept. of Commerce, 325 Broadway
Boulder, Colo. 80303

10. Project/Task/Work Unit No.
J0199115, Cont. of H0155008

11. Contract or Grant No.

12. Sponsoring Organization Name and Address
Office of the Assistant Director - Mining
Bureau of Mines
Dept. of the Interior
Washington, D.C. 20241

13. Type of Report
FINAL (Supplement)

14.

15. Supplementary Notes
This is a supplement to the Final Report of the same contract no. dated 1 May 1980.

16. Abstract

Abstract and Executive Summary: This report-supplement includes material that was completed only after the preparation of the mai- final report. We have also included the results of Modification No. 1 to Contract no. J0199115 dated 22 Jan. 1980. The following subjects are covered:

The views and conclusions contained in this document are those of the authors and should not be interpreted as necessarily representing the official policies or recommendations of the Interior Department's Bureau of Mines or of the U.S. Government.

17. Originator's Key Words	18. Availability Statement
Mine Communications Electromagnetics Mine Rescue Buried Loop R.F. Coupling	Unlimited

19. U.S. Security Classif. of the Report	20. U.S. Security Classif. of This Page	21. No. of Pages	22. Price
Unclassified	Unclassified	82	

PROPAGATION OF RADIO WAVES IN A COAL SEAM IN THE PRESENCE OF A CONDUCTING CABLE

by

David C. Chang and James R. Wait

ABSTRACT

The transmission of electromagnetic waves in an idealized coal seam or slab is analyzed for the case where an adjacent conductor is present. It is shown that the resultant attenuation is less than for the mode in a conductor-free seam. The approximations made are appropriate for low and medium frequencies.

I. INTRODUCTION

In mine communication at medium frequency range (1MHz or below), it has been observed that the attenuation of guided radio signals in a coal seam is substantially reduced in the presence of conducting rails and cables in the adjacent tunnel [Austin, 1978]. This fact is certainly consistent with the analysis by Wait and Hill [1974] for an axial conductor located anywhere inside a circular tunnel with lossy walls. A related analysis was carried out by Mahmoud and Wait [1974, 1976] for a rectangular tunnel wall. Such a phenomenon was also discussed by Lagace and Emslie [1978] in terms of the excitation efficiency of the induced current on a conducting rail or cable due to a vertical loop, but they did not actually calculate the propagation characteristics.

In this work, we consider the mathematical model of a thin wire (cable or rail) located inside a lossy dielectric slab tunnel (coal seam) of permittivity ε_1 and conductivity σ_1, and width$_1$ h. The slab is then surrounded by a highly conducting medium (rock or slate bed) of permittivity ε_2 and conductivity σ_2, as depicted in Figure 1. For a signal frequency of $\omega = 2\pi f$, the wave number of the tunnel medium is given by $k_1 = [-i\omega\mu_o(\sigma_1 + i\omega\varepsilon_1)]^{\frac{1}{2}}$ and that of the surrounding medium, $k_2 \simeq (-i\omega\mu_o\sigma_2)^{\frac{1}{2}} = (1-i)d_s^{-1}$ where d_s is defined as the skin depth. The complex propagation constant of the fundamental slab mode [Wait, 1971; Wait, 1976] in the absence of cables for nonzero h, is known to have a rather simple form

$$\frac{\Gamma_s}{k_1} \simeq \left(i\,\frac{2}{k_2 h} - 1\right)^{\frac{1}{2}} \qquad (1)$$

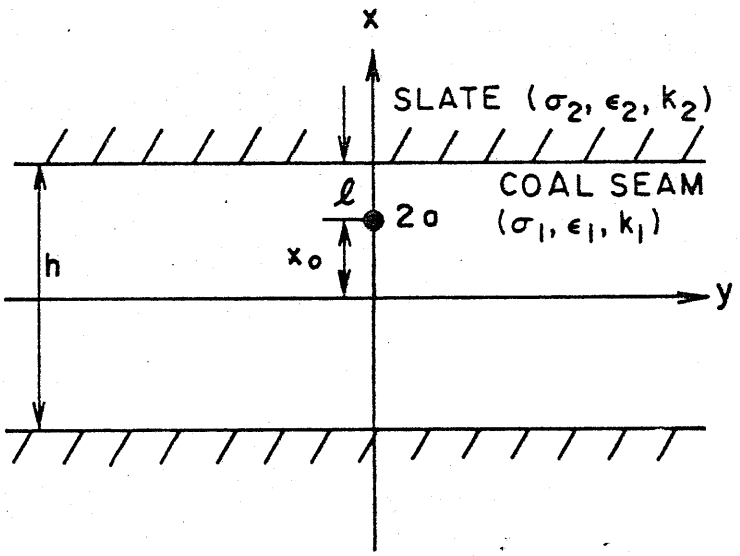

Figure 1

Basic slab configuration showing location of axial conductor, cable, pipe or rail in seam or tunnel.

when the conditions that $|k_2|^2 >> |k_1|^2$ and $k_1 h << 1$ are invoked. Provided that the width of the slab is small compared with the skin depth of the surrounding medium, the attenuation and propagation constants for this mode are found explicitly from (1) as $\Gamma_s = \alpha_s + i\beta_s$, where

$$\frac{\alpha_s}{k_1} \simeq \frac{\pi}{8}\left(\frac{d_s}{\sqrt{2}\, h}\right)^{\frac{1}{2}} \quad ; \quad \frac{\beta_s}{k_1} \simeq 0.85 \left(\frac{d_s}{\sqrt{2}\, h}\right)^{\frac{1}{2}} \tag{2}$$

on the assumption that k_1 is effectively real. Actually, (2) are rather crude approximations, but they illustrate very simply the functional dependence of the two parameters d_s and h. A more detailed discussion is given elsewhere [Wait, 1976], including the case where the slab width h approaches zero. The field distribution of this mode resembles that of a TEM-mode of a parallel-plate waveguide, with the exception that a significant amount of leakage into the surrounding medium may be possible when the width h is small compared to the skin-depth. Thus, the attenuation constant of this mode depends to a large extent on the penetration depth of the surrounding medium as indicated by (2).

The insertion of cables in the slab certainly will complicate the situation, since the field now has to redistribute itself in order to match the boundary conditions not only at the slab interface with the surrounding medium, but also on the cable surfaces. Depending upon the proximity of the cable to the slab, the amount of penetration into the surrounding medium can be very different, at least in principle. The purpose of this work is to investigate this specific problem.

II. AVERAGE AXIAL ELECTRIC FIELD ON A THIN-WIRE SURFACE

Our objective is to derive an expression for the attenuation and propagation constants, α and β, of a slab mode in the presence of a thin-wire which has a radius a and is at a distance x_o from the center (or a distance ℓ below the upper interface, as indicated in Figure 1). We first need to know the average axial field on the wire due to an equivalent current of the form $I_o \exp(i\omega t - \Gamma z)$ uniformly distributed on the wire surface. Later the complex propagation constant $\Gamma = \alpha + i\beta$ is to be determined.

Provided that we can invoke the thin-wire approximation, i.e. $\ell^2 >> a^2$ and $|k_1 a|^2 << 1$, the formal expression for the average axial field on the wire, as shown in Appendix A , consists of a primary field ψ^P and a secondary field ψ^S .

$$\langle E_z \rangle_{\rho=a} = \frac{-iI_o}{2\pi\omega\varepsilon_1^*} (\psi^P + \psi^S) \; ; \; \varepsilon_1^* = \varepsilon_1 - i(\sigma_1/\omega), \tag{3}$$

where

$$\psi^P \simeq (\Gamma^2+k_1^2)[\ell n(\Gamma^2+k_1^2)^{\frac{1}{2}} a + i\pi/2 + C - \ell n 2]; \; C = 0.5773, \tag{4}$$

$$\psi^S = \int_0^\infty \frac{d\lambda}{u_1(\lambda^2+\Gamma^2)} \left\{ [-\Gamma^2 u_1^2 R_e(\lambda) + k_1^2\lambda^2 R_m(\lambda)] e^{-u_1(h-2x_o)} \right.$$

$$+ \left[\frac{\Gamma^2 u_1^2 R_e(\lambda)}{1-R_e^2(\lambda)\exp(-2hu_1)} \{1 - R_e(\lambda) e^{-u_1(h-2x_o)}\}^2 \right.$$

$$\left. \left. + \frac{k_1^2\lambda^2 R_m(\lambda)}{1-R_m^2(\lambda)\exp(-2hu_1)} \right] \right\}$$

$$\cdot \{1 + R_m(\lambda)\, e^{-u_1(h-2x_o)}\}^2 \Big] e^{-u_1(h+2x_o)} \Big\}, \qquad (5)$$

$$R_e(\lambda) = \frac{k_2^2 u_1 - k_1^2 u_2}{k_2^2 u_1 + k_1^2 u_2} \quad ; \quad R_m(\lambda) = \frac{u_1 - u_2}{u_1 + u_2} \quad , \qquad (6)$$

$$u_j = (\lambda^2 - \Gamma^2 - k_j^2)^{\frac{1}{2}} \quad \text{and Re } u_j \geq 0 \text{ for } j = 1,2. \qquad (7)$$

The first term in the integrand of ψ^S , in the spectral domain, represents exactly the contribution of the partial image due to a line source located at a distance $\ell = h/2 - x_o$ above the upper surface. Together with the actual source, they yield a train of images (as a result of multiple reflections between the upper and lower interface), having a total contribution of the form given by the second term in the integrand.

Equation (5) as it stands obviously is too complicated to yield any physical insight regarding the behavior of ψ^S. However, simplification to the integral is possible with the assumption that the width of the coal seam is small compared with the skin-depth of the surrounding medium, i.e.,

$$|k_1|^2 h^2 < |k_2|^2 h^2 << 1 \qquad (8)$$

This is because the contribution to the integral in this case comes mainly from large λ where the two reflection coefficients R_e and R_m can be approximated by

$$R_e(\lambda) \simeq R_{eo} = \frac{k_2^2 - k_1^2}{k_2^2 + k_1^2} \quad ; \quad R_m(\lambda) \simeq 0. \tag{9}$$

The corresponding integral under this approximation is then given by

$$\psi_o^S = \Gamma^2 R_{eo} \int_0^\infty \frac{d\lambda}{u_1} \left\{ e^{-u_1(h-2x_o)} + e^{-u_1(h+2x_o)} \frac{[1 - R_{eo} e^{-u_1(h-2x_o)}]^2}{1 - R_{eo}^2 e^{-2u_1 h}} \right\} \tag{10}$$

which is evaluated analytically in Appendix B. From (B. 3), it is clear that ψ_o^S has only a rather weak, logarithmic dependence on h. Thus, unless the slab width is exceedingly small, one needs to retain the next higher order term in ψ^S , which is independent of h. To do that, we first subtract and add ψ_o^S from the expression of ψ^S in (5). The difference of the two is then evaluated at h = 0, so that $\psi^S = \psi_o^S + \delta$ and

$$\delta = \lim_{h \to 0} (\psi^S - \psi_o^S)$$

$$= 2\int_0^\infty \left\{ \left[\Gamma^2 u_1^2 \frac{R_e}{1 + R_e} - k_1^2 \lambda^2 \frac{R_m}{1 + R_m} \right] \frac{1}{\lambda^2 - \Gamma^2} - \Gamma^2 \left(\frac{R_{eo}}{1 + R_{eo}} \right) \right\} \frac{d\lambda}{u_1}$$

Interestingly, the integral actually can be carried out analytically once the relationship that

$$2[-\Gamma^2 u_1^2 \frac{R_e}{1+R_e} + k_1^2\lambda^2 \frac{R_m}{1-R_m}] = (\lambda^2 - \Gamma^2)[-\Gamma^2 - k_1^2 + \frac{u_1 k_1^2}{u_2 k_2^2}(k_2^2 + \Gamma^2)]$$

is recognized. Substitution of this expression into the integrand yields immediately

$$\delta = [k_1^2(\Gamma^2 + k_2^2)/k_2^2] \ln\left(\frac{\Gamma^2 + k_2^2}{\Gamma^2 + k_1^2}\right)^{\frac{1}{2}} \tag{11}$$

which can then be combined with the expression for ψ_o^S in (B.3) and ψ^P in (4) to give a delightfully simple result for the axial field on the cable surface as

$$\langle E_z \rangle_{\rho=a} \simeq \frac{-iI_o}{2\pi\omega\varepsilon_1^*}\left\{(k_1^2 + \Gamma^2)\ln\frac{2h}{a} + \Gamma^2\Omega_o - \frac{k_1^2}{k_2^2}(k_2^2 + \Gamma^2)\ln[(k_2^2 + \Gamma^2)^{\frac{1}{2}}h] + i\frac{\pi}{2} + C\right\}$$

where the parameter Ω_o is given by (B.4) as

$$\Omega_o = R_{eo}\ln\Delta + \sum_{m=1}^{\infty} R_{eo}^{2m-1}[\ln(m-\Delta) - 2R_{eo}\ln m + R_{eo}^2\ln(m+\Delta)] \quad ; \quad \Delta = \ell/h \tag{13}$$

and, therefore, involves only the geometric ratio of ℓ and h, and R_{eo}. It is of interest to note that the derivation leading to (12) so far only involves the assumption of $|k_2|^2 h^2 << 1$ and $\ell^2 >> a^2$. In actual application, the additional condition that $|k_2|^2 >> |k_1|^2$ also applies so that (12) and (13) can be further simplified to

$$\langle E_z \rangle_{\rho=a} \simeq \frac{-i I_o}{2\pi\omega\varepsilon_1^*} \left\{(k_1^2 + \Gamma^2)\ \ell n \frac{2\ell_e}{a} - k_1^2 [\ell n(ik_2\ell_e) + C]\right\} \tag{14}$$

$$\simeq \frac{+iI_o}{2\pi\omega\varepsilon_1^*} \left\{-\Gamma^2 \ell n\ \frac{2\ell_e}{a} + k_1^2 [\ell n(ik_2 a/2) + C]\right\} \tag{15}$$

with the effective height ℓ_e defined as

$$\ell_e = h\, e^{\Omega_o} \simeq \ell \exp\left(\sum_{m=1}^{\infty} \ell n \frac{m^2 - \Delta^2}{m^2}\right)$$

$$\simeq \ell \exp\left(-\frac{\pi^2\Delta^2}{6}\right); \quad \Delta = \ell/h\ . \tag{16}$$

The result, as given by (14), is identical in form with the case of a thin-wire located at a distance ℓ_e above a conducting half-space [Chang and Wait, 1974]. Since the actual distance to the upper interface is ℓ and $\ell_e/\ell = \exp(-\pi^2\Delta^2/6) < 1$ according to (16), one might conclude that the net effect of the interaction between upper and lower interfaces is to bring the cable a little closer to the upper interface. Obviously, the periodic nature of the partial "images" in the spectral domain is insignificant in the spatial domain when the tunnel width is small compared with the skin-depth.

III. ATTENUATION AND PROPAGATION IN A CABLE-TUNNEL SYSTEM

For the case of a cable which is located inside a coal seam, having a known series impedance Z_i, the complex propagation constant Γ of the fundamental mode can be obtained by enforcing the boundary condition on the cable surface. Because we have assumed the cable radius is small, we can replace equivalent current I_o by $2\pi a$ times the average angular magnetic field, $\langle H_\phi \rangle$. The use of the impedance condition, $\langle E_z \rangle = 2\pi a Z_i \langle H_\phi \rangle$ and (15) then provides an appropriate expression for Γ as follows:

$$\Gamma^2 \ell n \frac{2\ell_e}{a} + i\omega\varepsilon_1^* [i\omega\mu_o(\ell n i k_2 a/2 + C) + 2\pi Z_i] = 0 \tag{16}$$

or

$$\Gamma^2 = YZ \tag{17}$$

where

$$Y = i2\pi\omega\varepsilon_1^* [\ell n 2\ell_e/a]^{-1} \tag{18}$$

and

$$Z = -i\omega\mu_o (2\pi)^{-1} [\ell n (ik_2 a/2) + C] + Z_i \tag{19}$$

Equation (17) resembles that for a lossy transmission-line system, with Z,Y being the distributed series impedance and shunt admittance, respectively. Since we have assumed that the slab (coal seam) width is very small compared with the skin-depth, it is not surprising to see that the series impedance Z consists mainly of the self-inductance of the cable immersed in the ambient medium (slate), and the surface impedance Z_i. On the other hand, because of the high conductivity contrast between the slate and the coal seam, the shunt admittance is essentially that of a wire located in a perfectly-conducting parallel-plate region. As we mentioned before, the series of images produced by the multiple reflection between the two plates results in an apparent image at a distance $2\ell_e$ away from the cable itself. For a conducting rail, $Z_i = 0$ so that

$$\frac{\Gamma}{k_1} = \left[\frac{\ell n(ik_2 a/2) + C}{\ell n \frac{2\ell_e}{a}}\right]^{\frac{1}{2}} ; \quad \ell_e = \ell e^{-(\pi \ell/h)^2/6)} \tag{20}$$

Comparison of (20) with (1) now enables us to assess the importance of the conducting rails and cables in mine communication. It is clear that, in the absence of these conductors, waves are guided by the upper and lower surfaces of the coal seam with the surrounding medium. Thus, the width of the slab compared with the skin-depth determines the extent of penetration into the surrounding medium, and hence the attenuation as well as the phase constants. With the presence of a parallel conductor, however, the field concentration is largely controlled by the size of the conductor because a substantial amount of longitudinal current can now flow on the conductor surface and the surrounding medium acts more like a return path. As an extreme case, the propagation constant approaches to the value corresponding to the wave number of the medium in the immediate vicinity of the conductor in the limit of a vanishingly small radius. As is evident by the dependence of h in (20) the width of the slab also becomes a relatively less important parameter in determining the attenuation and phase constants. Instead it is the ratio of the radius and height of the conductors. Dependence on height compared with the skin depth of the surrounding medium is also rather weak because of the logarithmic nature of this dependence. In fact, the attenuation and propagation constants can be explicitly derived from (20) as $\Gamma = \alpha_c + i\beta_c$, with

$$\frac{\alpha_c}{k_1} = \frac{\pi - 2\phi_2}{4(L_a L_b)^{\frac{1}{2}}} ; \quad \frac{\beta_c}{k_1} = \left(\frac{L_a}{L_b}\right)^{\frac{1}{2}} \tag{21}$$

where $L_a = -(\ell n|k_2|a/2 + C)$, $L_b = \ell n(2\ell_e/a)$, and $k_2 = |k_2| \exp(-i\phi_2)$ where ϕ_2 is a phase angle. Again k_1 is assumed real.

To illustrate the nature of the results, we show in Fig. 2 a comparixon for the case with and without the conductor. The attenuation constant is plotted as a function of frequency for a special case where the seam width h = 3m, and the conductor is distance ℓ = 1m from the seam surface, the radius of the conductor a = 0.02m. The conductivity σ_2 of the bounding material (i.e., slate) is 2×10^{-2}mhos/m. The dashed line is for the case when the conductor is absent as computed from (2), and the solid line is when the conductor is present as computed from (20). For the latter case, the values based upon a numerical evaluation of the exact expression as given in (3)-(5) are also included. From the figure, it is clear that for frequencies of practical interest, attenuation of the guided electromagnetic waves is indeed substantially reduced as a result of the conducting rail's presence.

Actually, for the results shown in Fig. 2, the seam was replaced by free space but the results apply qualitatively for an effectively lossless seam of any permittivity if distances are scaled accordingly, e.g., $k_1 d$ and $k_2 d$ are fixed. Of course, the theory presented is valid for a dissipative seam where σ_1 is comparable with the displacement term $\varepsilon_1 \omega$ but we do not show such results here.

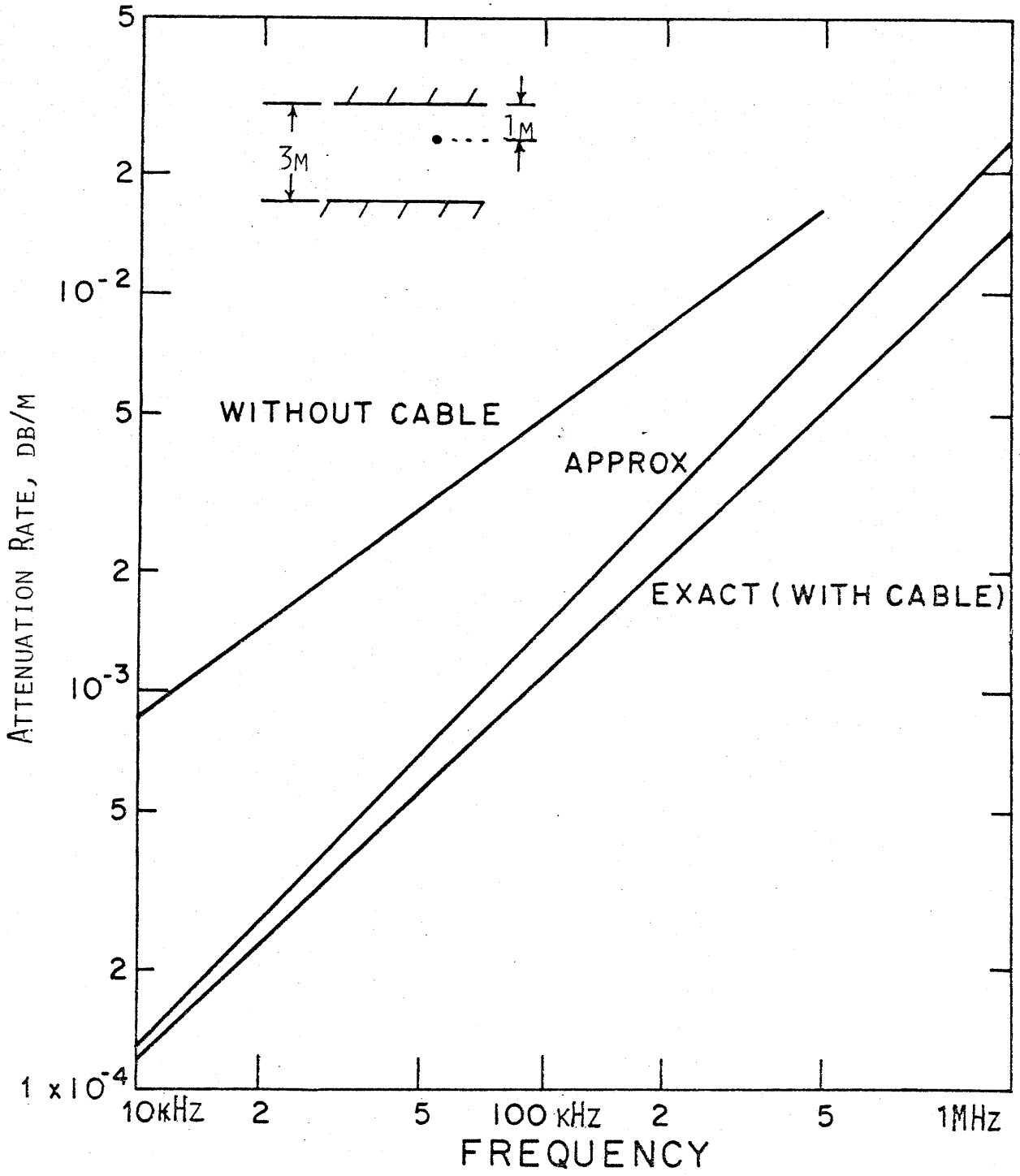
5
2
10-2
5
2
10-3
5
2
1 x 10-4
ATTENUATION RATE, DB/M
3M
1M
WITHOUT CABLE
APPROX
EXACT (WITH CABLE)
10KHZ
2
5
100 KHZ
2
5
1MHZ
FREQUENCY

Figure 2

APPENDIX A

Derivation of Axial Field Expressions

Here we derive an expression for the axial electric field at the surface of a thin wire carrying a filamental current $I_o \exp(-\Gamma z)$. The relevant geometry is indicated in Fig. 1. Following an earlier formulation for a similar problem [Wait, 1977], it is a fairly simple matter to derive explicit expressions for the x directed electric and magnetic Hertz vectors within the slab region. These so-called electric and magnetic Hertz potentials π_e and π_m must be of the respective forms:

$$\pi_e = \frac{-i\Gamma I_o}{4\pi\omega\varepsilon_1^*} \int_{-\infty}^{\infty} (\bar{+}e^{\bar{+}u_1(x-x_o)} + A_e e^{u_1 x} + B_e e^{-u_1 x}) e^{-i\lambda y} \frac{d\lambda}{\lambda^2 - \Gamma^2} \qquad (A.1)$$

$$\pi_m = \frac{iI_o}{4\pi} \int_{-\infty}^{\infty} (e^{\bar{+}u_1(x-x_o)} + A_m e^{u_1 x} + B_m e^{-u_1 x}) e^{-i\lambda y} \frac{\lambda d\lambda}{u_1(\lambda^2 - \Gamma^2)} \qquad (A.2)$$

where $\varepsilon_1^* = \varepsilon_1 - i(\sigma_1/\omega)$ and where $(\bar{+})$ designates the region $x \lesseqgtr x_o$; A_e, B_e and A_m, B_m are as yet undetermined constants. However, since in the region $x > x_o$, B_e, B_m are part of the incoming wave that are incident onto the upper interface and A_e, A_n are the reflected wave, we have

$$A_e e^{u_1 h/2} = R_e(-e^{u_1 x_o} + B_e) e^{-u_1 h/2} \qquad (A.3)$$

$$A_m e^{u_1 h/2} = R_m(e^{u_1 x_o} + B_m) e^{-u_1 h/2} \qquad (A.4)$$

where R_e and R_m are as defined by (6).

Likewise, for the lower interface

$$B_e e^{u_1 h/2} = R_e(e^{-u_1 x_o} + A_e) e^{-u_1 h/2} \qquad (A.5)$$

$$B_m e^{u_1 h/2} = R_m(e^{-u_1 x_o} + A_m) e^{-u_1 h/2} \qquad (A.6)$$

Using (A.3) to (A.6), we solve for the A's and B's:

$$A_{e,m} = R_{e,m}\, e^{-2u_1 h}\left[\frac{R_{e,m}\, e^{-u_1 x_o} + e^{u_1(x_o+h)}}{1 - R_{e,m}^2\, e^{-2u_1 h}}\right] \tag{A.7}$$

$$B_{e,m} = R_{e,m}\, e^{-2u_1 h}\left[\frac{\mp R_{e,m}\, e^{u_1 x_o} + e^{u_1(h-x_o)}}{1 - R_{e,m}^2\, e^{-2u_1 h}}\right] \tag{A.8}$$

Substitution of (A.7) and (A.8) into (A.3) to (A.6) then yield the expression for π_e and π_m. To obtain the axial electric field, we only need to use the relationship

$$E_z = \frac{\partial^2}{\partial x\, \partial z}\,\pi_e + i\omega\mu_o \frac{\partial}{\partial y}\,\pi_m$$

to obtain from (A.3) to (A.6) the following expression

$$E_z = \frac{iI_o}{4\pi\omega\varepsilon_1}\left[(k_1^2+\Gamma^2)\int_{-\infty}^{\infty} e^{\mp u_1(x-x_o)}\, e^{-i\lambda y}\,\frac{d\lambda}{u_1}\right.$$

$$+ 2\int_{\infty}^{\infty}\frac{1}{\lambda^2-\Gamma^2}\left\{\frac{+\Gamma^2 u_1^2 R_e}{\Delta_e}\left[R_e e^{-2u_1 h}\cosh u_1(x-x_o) - e^{-u_1 h}\cosh u_1(x+x_o)\right]\right.$$

$$\left.\left. + \frac{k_1^2\lambda^2 R_m}{\Delta_m}\left[R_m e^{-2u_1 h}\cosh u_1(x-x_o) + e^{-u_1 h}\cosh u_1(x+x_o)\right]\right\}\right]; \tag{A.9}$$

where

$$\Delta_{e,m} = 1 - R_{e,m}^2\, e^{-2u_1 h} \tag{A.10}$$

In deriving (A.9), the identity $\Gamma^2 u_1^2 + \lambda^2 k_1^2 = (\lambda^2 - \Gamma^2)(k_1^2 + \Gamma^2)$ was used in obtaining the first integral which is known to be $2K_o(ir[\Gamma^2+k_1^2]^{\frac{1}{2}})$; $r = [(x-x_o)^2 + y^2]^{\frac{1}{2}}$ and K_o is the modified Bessel function of the

second kind. On the wire surface, the average axial field is then obtained by setting $r = a$, $x = x_o$ and $y = 0$:

$$\langle E_z \rangle_{\rho=a} = \frac{iI_o}{2\pi\omega\varepsilon_o} \left\{ (k_1^2 + \Gamma^2) K_o(ia[\Gamma^2+k_1^2]^{\frac{1}{2}}) \right.$$

$$+ \int_o^\infty \left[\frac{+\Gamma^2 u_1^2 R_e}{\Delta_e} (R_e e^{-u_1 h} - \cosh 2u_1 x_o) + \frac{k_1^2 \lambda^2 R_m}{\Delta_m} (R_m e^{-u_1 h} \right.$$

$$\left. \left. + \cosh 2u_1 x_o) \right] e^{-u_1 h} \frac{d\lambda}{(\lambda^2 - \Gamma^2)} \right\} \qquad \text{(A.11)}$$

Provided the radius is small, K_o can be approximated by $-\ell n[ia(\Gamma^2+k_1^2)^{\frac{1}{2}}]$. On the other hand, the terms inside the square bracket can be rearranged according to

$$R_{e,m}(R_{e,m} e^{-u_1 h} \mp \cosh 2u_1 x_o) = \mp R_{e,m} e^{-u_1 (h-2x_o)}$$

$$\mp \frac{R_{e,m} e^{-u_1 (h+2x_o)}}{1 - R_{e,m}^2 e^{-2hu_1}} [1 - R_{e,m} e^{-u_1 (h-2x_o)}]^2 \qquad \text{(A.12)}$$

where the upper sign is for the R_e and lower sign for R_m. Substitution of (A.12) into (A.11) yields immediately the expressions given in (3) - (5).

APPENDIX B

Evaulation of E^s_{zo}

The integral given in (10) is evaluated in this appendix. Recognizing that $|R_{eo} \exp(-2u_1 h)| < 1$, we can first expand the denominator in series to obtain

$$e^{-u_1(h+2x_o)}\,\frac{[1-R_{eo}\,e^{-u_1(h-2x_o)}]^2}{1-R_{eo}^2\,e^{-2u_1h}} = \sum_{m=0}^{\infty} R_{eo}^{2m}\,e^{-2mu_1h}$$

$$\left\{e^{-u_1(h+2x_o)} - 2R_{eo}\,e^{-u_1h} + R_{eo}^2\,e^{-u_1(3h-2x_o)}\right\}$$

so that each term in the series can be integrated analytically according to the identity

$$K_o(x[\Gamma^2+k_1^2]^{\frac{1}{2}}) = \int_0^{\infty} e^{-u_1x}\,\frac{d\lambda}{u_1} \quad .$$

Consequently, we obtain from (10) the alternative expression

$$\psi_o^s = \Gamma^2 R_{eo}\Big[K_o(\zeta_1[h-2x_o]) + \sum_{m=0}^{\infty} R_{eo}^{2m}\{K_o([(2m+1)h+2x_o]\zeta_1) - 2R_{eo}K_o(2[m+1]h\zeta_1) + R_{eo}^2K_o([(2m+3)h-2x_o]\zeta_1)\}\Big] \qquad (B.1)$$

where $\zeta_1 = i(\Gamma^2+k_1^2)^{\frac{1}{2}}$. Now since we have assumed the seam size is small compared with the guided wavelength as well as the wavelength of the medium, $|\zeta_1|h$ generally is much smaller than 1. A small-argument expansion of K_o then yields approximately,

$$E_{zo}^s = -\Gamma^2\,R_{eo}\left[\left(\frac{2}{1+R_{eo}}\right)\left[\ell n\ 2h(\Gamma^2+k_1^2)^{\frac{1}{2}}\,i\pi/2 + C - \ell n2\right] + \ell n(h-2x_0)/2h\right.$$

$$+ \sum_{m=1}^{\infty} R_{eo}^{2(m-1)} \{\ell n[(2m-1)h+2x_o]/2h - 2R_{eo}\, \ell n\, m$$

$$+ R_{eo}^2 \ell n[(2m+1)h-2x_o]/2h\}\Big] \qquad (B.2)$$

Defining $\Delta = \ell/h = (\frac{1}{2} - \frac{x_o}{n})$ as the ratio of the distance to the upper boundary and the tunnel width and using the explicit expression of R_{eo} in (9), we have from (B.2) the simplified result

$$E_{zo}^s = -\Gamma^2 \left[\frac{k_2^2-k_1^2}{k_2^2}\right][\ell n 2h(\Gamma^2+k_1^2)^{\frac{1}{2}} + i\pi/2 + C - \ell n 2] - \Gamma^2\Omega_o \qquad (B.3)$$

where $\Omega_o = R_{eo}\, \ell n\Delta + \sum_{m=1}^{\infty} R_{eo}^{2m-1} [\ell n(m-\Delta) - 2R_{eo}\, \ell n\, m + R_{eo}^2\, \ell n(m+\Delta)]$ (B.4)

Expression (B.3) can then be used with the expression δE derived in (11), and E_z^P in (4) to obtain the total axial electric field expression given in (12).

References

Abramovitz, M. and I.A. Stegun [1964], Handbook of Mathematical Functions, Chapter 9, Dover.

Austin, B.A. [1978], "Underground radio communication techniques and systems in South African mines," Proc. Electromagnetic Guided Waves in Mine Environments (ed. J.R. Wait), p. 87-99, CIRES, Univ. of Colorado, Boulder, CO, [U.S. Bureau of Mines Contract No. H0 5008, Open File Report No.

Chang, D.C. and J.R. Wait [1974],"Extremely low frequency propagation along a horizontal wire located above or buried in the earth," IEEE Tran. Comm., vol. COM-22, 4, 421-428.

Lagace, R.L. and A.G. Emslie [1978], "Coupling of the seam mode to a cable in a tunnel at medium radio frequencies," n. Rept. under USBM Contract H0346045 to A.D. Little, Inc. Cambr e, Mass.

Plate, S.W., D.C. Chang and E.F. Kuester [1978], "Propagating modes on a buried leaky coaxial cable," Sci. Rept. #32, Electromagnetics Laboratory, University of Colorado, Boulder, CO.

Wait, J.R. [1971], "Note on calculations of propagation parameters for an idealized earth-crust waveguide," Geophysical Monograph, No. 14, (ed. J.G. Heacock), vol. 14, 325-331, (published by Amer Geophys. Union).

Wait, J.R. and D.A. Hill [1974], "Guided electromagnetic waves along an axial conductor in a circular tunnel," IEEE Trans. APS, vol. AP 22, 4, 627-630.

Wait, J.R. [1976], "Note on the theory of transmission of electromagnetic waves in a coal seam," Radio Science, vol. 11, 4, 63-265.

Wait, J.R. [1977], "Excitation of an ensemble of paral cables by an external dipole over a layered ground," Arch. Elek bertrangungs-tech., vol. 31, 489-493.

Mahmoud, S.F., and Wait, J.R. [1974], "Theory of Wave pagation along a thin wire inside a rectangular waveguide," Radio Sc nce, Vol. 9, 3, 417-420.

Mahmoud, S.F., and Wait, J.R. [1976], "Calculated chann characteristics of a braided coaxial cable in a mine tunnel," I.E.E.E. rans. Comm., Vol. COM-24, 1, 82-87.

Calculated Estimate of R.F. Coupling From a Trolley Wire and Blasting Cap Circuit

by
D.A. Hill and J.R. Wait

Following a query from the sponsor, we have considered an idealized model of the radio frequency coupling from the trolley wire to an adjacent circuit. Our objective is to deduce the current I_a that could be injected into a parallel wire of length ℓ grounded through resistors R at the end points. Such a current I_a could constitute a hazard if such a circuit is part of an electric detonator system.

The model we adopt is depicted in Fig. 1. The tunnel cross-section is semi-circular with radius a_o and is bounded by homogeneous rock of conductivity σ_e and by a ground plane which is taken to be perfectly conducting. The trolley wire I_o is located at (ρ_o, ϕ_o) in terms of cylindrical coordinates while the detonator circuit is located at (ρ_a, ϕ_a).

In the absence of the detonator circuit, we can employ a previous formulation [1] to determine the fields everywhere within the tunnel for a specified current on the trolley wire of radius c and conductivity σ_w. Of special interest here is the transmission-line type mode in which we have the lowest attenuation, although the formulation could be used for other modes that may be important at V.H.F.

The axial electric field E_{oz} at point A is thus given by

$$E_{oz} = - \frac{\eta_o v^2 I_o}{2\pi\gamma_o} [K_o(v\rho_d^+) - S^+ - K_o(v\rho_d^-) + S^-]e^{-\Gamma z}$$

where

---

[1] D.A. Hill and J.R. Wait, "Analysis of radio frequency transmission along a trolley wire in a mine tunnel", *IEEE Trans. Electromagn. Compat.*, Vol. EMC-18, No. 4, pp. 170-174, Nov. 1976.

$$S^{\pm} = \sum_m R_m \frac{K_m(va)}{I_m(va)} I_m(v\rho_o) I_m(v\rho_a) \exp[-im(\phi_a \mp \phi_o)]$$

and

$$\rho_d^{\pm} = [\rho_o^2 + \rho_a^2 - 2\rho_o\rho_a \cos(\phi_a \mp \phi_o)]^{\frac{1}{2}} \quad \text{and} \quad v = (\gamma_o^2 - \Gamma^2)^{\frac{1}{2}}.$$

The notation is identical to that given in the referenced paper [1]. We can actually invoke the quasi-static approximation

$$\frac{K_m(va_o)}{I_m(va_o)} I_m(v\rho_o) I_m(v\rho_a) \simeq \begin{cases} (\rho_o\rho_a/a_o^2)^{|m|} & ; \quad m \neq 0 \\ -\ell n(va_o) & ; \quad m = 0 \end{cases}$$

Here we are assuming that the current is I_o amps at the reference point $z = 0$. Also, Γ is the (complex) propagation constant of the desired mode, and γ_o and η_o are the propagation constant and the intrinsic impedance of free space.

Now, the parallel detonator circuit has a length ℓ small compared with $|\Gamma|^{-1}$; thus it is a very good approximation to say that the driving voltage in the secondary circuit is ℓE_{az} evaluated at $z = 0$. Then the resulting current $I_a \simeq \ell E_{oz}/2R$ where R is the value of the terminating resistors. This neglects the self inductance of the circuit which is justified in the present context.

A selection of parameters were made that would seem to encompass most cases of practical interest. Using these parameters (indicated in Table I), the axial field $|E_{az}|$ in milli-volts/m and the driven current $|I_a|$ in milli-amps are shown for a driven current I_o of 1 amp.

The driven current values can, of course, be easily re-calculated for any other grounded resistance R. The 10 ohm value indicated is "nominal".

As o_a become small, the field diminishes in roughly linear proportion. In fact, it is really the area traced out by the detonator wire and its image in the ground plane that should be minimized. Correspondingly, if the detonator circuit is fully closed (i.e. not grounded), the hazard current I_a will be approximately proportional to the total enclosed area.

Also, it is evident that, for everything else held constant, the hazard current I_a is roughly proportional to frequency.

TABLE 1

Trolley Line Field (E_{az}) and Hazard Current (I_a).

Frequency (kHz)	ϕ_a	ρ_a (m)	$\lvert E_{az} \rvert$ (mV/m)	$\lvert I_a \rvert$ (mamp)
50	45°	0.1	2.33	1.17
"	"	0.2	4.50	2.24
"	"	0.5	10.04	5.02
"	"	1.0	16.45	8.23
"	90°	0.1	3.42	1.71
"	"	0.2	6.83	3.41
"	"	0.5	16.94	8.47
"	"	1.0	32.93	16.47
"	135°	0.1	2.50	1.25
"	"	0.2	5.19	2.59
"	"	0.5	14.34	7.17
"	"	1.0	33.45	16.73
100	45°	0.1	4.66	2.33
"	"	0.2	8.98	4.49
"	"	0.5	20.05	10.03
"	"	1.0	32.85	16.43
"	90°	0.1	6.83	3.41
"	"	0.2	13.64	6.82
"	"	0.5	33.84	16.92
"	"	1.0	65.79	32.89
"	135°	0.1	5.00	2.50
"	"	0.2	10.36	5.18
"	"	0.5	28.66	14.33
"	"	1.0	66.86	33.43
200	45°	0.1	9.28	4.64
"	"	0.2	17.90	8.95
"	"	0.5	39.95	19.97
"	"	1.0	65.42	32.71
"	90°	0.1	13.60	6.80
"	"	0.2	27.17	13.59
"	"	0.5	67.42	33.71
"	"	1.0	131.07	65.54
"	135°	0.1	9.97	4.98
"	"	0.2	20.65	10.32
"	"	0.5	57.12	28.56
"	"	1.0	133.27	66.64

$a_o = 2m$, $\varepsilon_e/\varepsilon_o = 10$, $\sigma_e = 10^{-3}$mho/m, $\phi_o = 135°$, $\rho_o = 1.8m$, $c = 1.5cm$, $\sigma_w = 5.7 \times 10^{7}$mho/m, $I_o = 1$ amp, $\ell = 10$ m, $R = 10$ ohms.

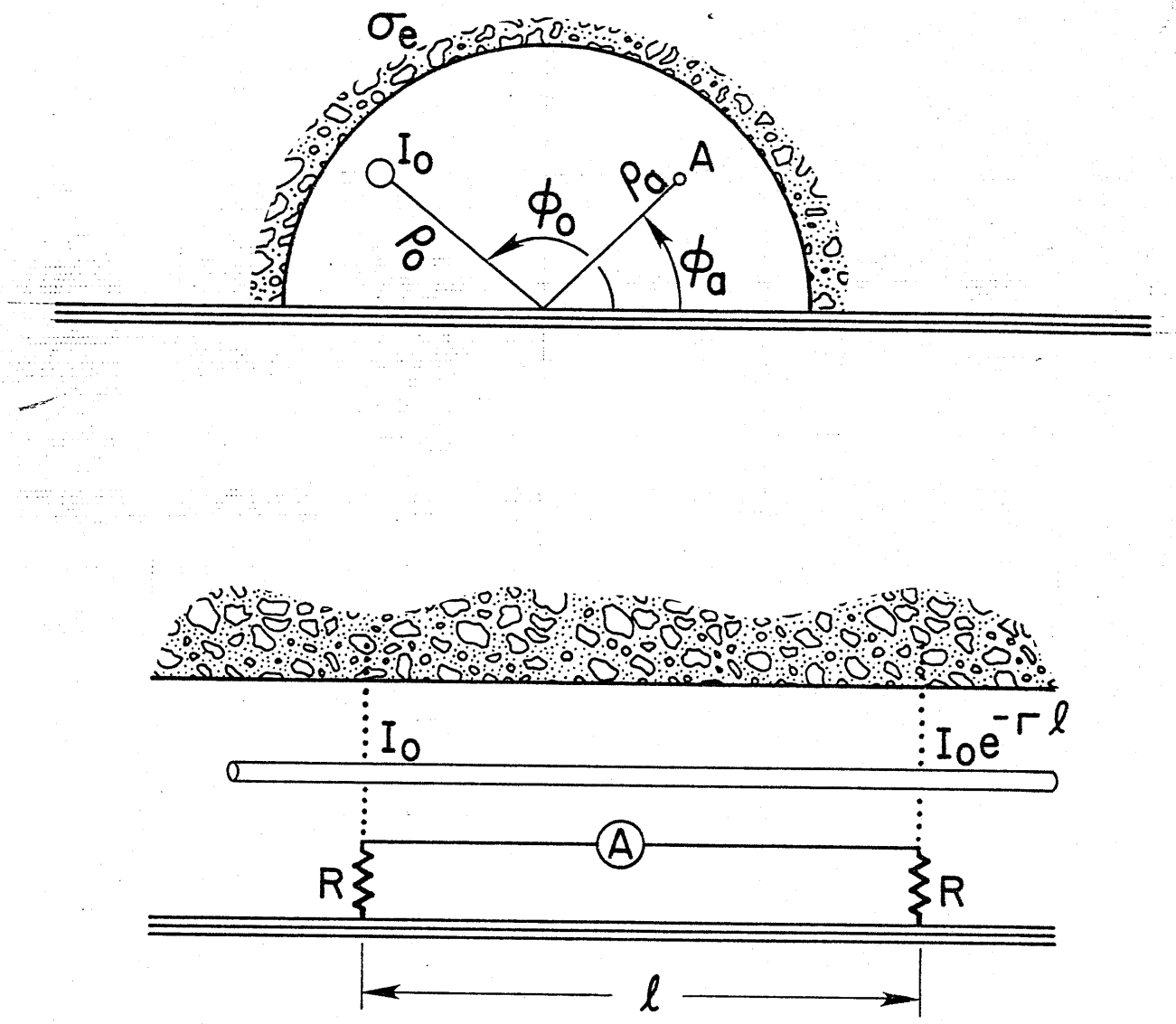

Fig. 1 Semi-circular tunnel model showing location of axial trolley wire, carrying a current I_o, and parallel detonator circuit of length ℓ.

ANALYSIS OF A TUNNEL WAVEGUIDE JUNCTION

by

David A. Hill
Institute for Telecommunication Sciences/
National Telecommunications and Information Administration

and

James R. Wait
Environmental Research Laboratories
National Oceanic and Atmospheric Administration
Cooperative Institute for Research in Environmental Sciences

U.S. Department of Commerce
325 Broadway, Boulder, Colorado 80309

Abstract - The two-dimensional model of intersecting tunnels with impedance walls is analyzed by a three-region mode matching technique. The numerical solution is found to converge smoothly, and numerical checks on power conservation, reciprocity, and the edge condition are well satisfied. A general result is that the lowest order mode is efficient in exciting the higher order mode in the crosscut tunnel, but is not efficient in exciting the lowest order mode.

INTRODUCTION

Underground coal mines are typically extensive labyrinths of parallel tunnels and right angle crosscuts [Murphy and Parkinson, 1978]. Consequently, tunnel junctions can have a significant effect on radio communication in mines. EM propagation in straight tunnels and around corners has been studied by Emslie, Lagace and Strong [1975]. They employed an ingenious approximate approach that lumped all the higher order waveguide modes into a single "diffuse" component. Here we employ rigorous modal expansions for the fields, and the higher order waveguide modes are considered explicitly. However, the price we pay is that the model, by necessity, is highly idealized.

We adopt two-dimensional geometry with a single tunnel junction of two infinitely-long tunnels as shown in Figure 1. The geometry is similar to that encountered in some waveguide junction problems except that we allow the tunnel walls to have nonzero surface impedances. Thus, the attenuation of the waveguide modes is allowed for. A separate expansion in terms of cavity modes is utilized in the junction region. Then matching is employed at the cavity-waveguide boundaries. The coefficients of the cavity modes are eliminated analytically, and the coefficients of the waveguide modes are obtained numerically through matrix inversion.

The incident field can be any one of the waveguide modes, and the resulting transmitted and reflected mode coefficients define a scattering matrix (Kerns and Beatty, 1967) for the junction. Checks on the numerical solution are obtained by examining power conservation, reciprocity, and the edge condition.

WAVEGUIDE MODE FORMULATION

The tunnel junction configuration shown in Figure 1 is symmetric in both x and y. Consequently by employing either symmetric or antisymmetric excitation, we can reduce the analysis to one quadrant which is bounded either by electric or magnetic walls. The case where the fields are symmetric in both x and y is of greatest interest because the lowest order symmetric mode has the lowest attenuation. Thus, we replace the geometry in Figure 1 by the equivalent geometry in Figure 2. In order to actually handle the most general excitation, it would be necessary to solve four geometries similar to that in Figure 2 and use superposition of the four solutions.

The geometry in Figure 2 is invariant in the z direction, and the magnetic walls in the yz and xz planes ensure the even symmetry in y and x.

The tunnels are of half-widths a and b, and the tunnel walls have surface impedances Z_a and Z_b. The region bounded by the tunnel walls and the magnetic walls has free space permittivity ε_o and permeability μ_o. The electric field is chosen to have only a z component from which the magnetic field components can be determined. Thus, we are solving a scalar problem, and E_z satisfies the scalar wave equation in all three regions

$$(\nabla^2 + k^2)E_z = 0 \ , \tag{1}$$

where $k^2 = \omega^2\mu_o\varepsilon_o$ and $e^{i\omega t}$ time dependence is assumed. We choose the E_z polarization because no TEM modes are then supported by the waveguide regions 1 and 2. Thus the results are more representative of the three dimensional problem [Emslie, Lagace and Strong, 1975] where no TEM modes whatsoever are possible.

We designate three regions in Figure 2 because the waveguide mode expansions which are valid in regions 1 and 2 cannot be continued analytically into the cavity region 3 [Lewin, 1970]. Thus, we employ a general expansion in rectangular cavity modes in region 3. This is similar to the approach for waveguide circulators where a circular cavity region accommodates arbitrary waveguide intersection angles [Copplestone, 1979].

We assume an arbitrary mode m of unity strength for the incident field in region 1 and an infinite series of reflected modes of unknown strength $R_{n,m}$. Thus, the total electric field in region 1, E_{1z}, can be written

$$E_{1z} = \cos(kC_m x)\cos(kS_m y) + \sum_{n=1}^{\infty} R_{n,m}\cos(kC_n x)e^{-ikS_n y} \ , \tag{2}$$

where C_n and S_n are determined from the modal equation for an infinite guide. We may visualize the incident field $\cos(kS_m y)$ as the superposition of incoming and outgoing modes, $\exp(ikS_m y)$ and $\exp(-ikS_m y)$, as required for symmetric excitation.

In any region the magnetic field components H_x and H_y are determined from E_z by

$$H_x = \frac{-1}{i\omega\mu_o}\frac{\partial E_z}{\partial y} \quad \text{and} \quad H_y = \frac{1}{i\omega\mu_o}\frac{\partial E_z}{\partial x} . \tag{3}$$

From (2) and (3), the magnetic field components in region 1 are given by

$$H_{1y} = \frac{k}{i\omega\mu_o}\left[S_m \cos(kC_m x)\sin(kS_m y) + \sum_{n=1}^{\infty} iS_n R_{n,m}\cos(kC_n x)\exp(-ikS_n y)\right] \tag{4}$$

and

$$H_{1x} = -\frac{-k}{i\omega\mu_o}\left[C_m \sin(kC_m x)\cos(kS_m y) + \sum_{n=1}^{\infty} C_n \sin(kC_m x)\exp(-ikS_n y)\right] \tag{5}$$

Note that H_{1y} is zero at $x = 0$ as required by the boundary condition at the magnetic wall. Also in order to satisfy the scalar wave equation we have

$$C_n^2 + S_n^2 = 1 . \tag{6}$$

At $x = a$, we apply the impedance boundary condition

$$\left.\frac{E_{1z}}{H_{1y}}\right|_{x=a} = -Z_a . \tag{7}$$

This condition results in a modal equation for C_n whose solution is discussed in Appendix A.

In region 2 we have only outgoing modes of unknown strength $Q_{n,m}$, and the field components can be written

$$E_{2z} = \sum_{n=1}^{\infty} Q_{n,m}\cos(k\hat{C}_n y)\exp(-ik\hat{S}_n x) , \tag{8}$$

$$H_{2x} = \frac{k}{i\omega\mu_o}\sum_{n=1}^{\infty}\hat{C}_n Q_{n,m}\sin(k\hat{C}_n y)\exp(-ik\hat{S}_n x) , \tag{9}$$

and

$$H_{2y} = \frac{k}{\omega\mu_o}\sum_{n=1}^{\infty}\hat{S}_n Q_{n,m}\cos(k\hat{C}_n y)\exp(-ik\hat{S}_n x) , \tag{10}$$

where

$$\hat{C}_n^2 + \hat{S}_n^2 = 1 \tag{11}$$

The impedance condition is applied at $y = b$:

$$\left.\frac{E_{2z}}{H_{2x}}\right|_{y=b} = Z_b . \tag{12}$$

This condition again results in a mode equation for $\hat{C}_n$ as discussed in Appendix A.

CAVITY MODE FORMULATION

In region 3, we require a general cavity mode expansion which yields $H_{3x} = 0$ at $y = 0$ and $H_{3y} = 0$ at $x = 0$. By generalizing the expansion for a magnetic wall cavity with one open side as given by Morse and Feshbach [1953] to the case of two open sides, we obtain

$$E_{3z} = \sum_{n=0}^{\infty} A_n \cos\left(\frac{n\pi x}{a}\right) \cos(k_{yn} y) + \sum_{n=0}^{\infty} B_n \cos\left(\frac{n\pi y}{b}\right) \cos(k_{xn} x) , \tag{13}$$

$$H_{3x} = \frac{1}{i\omega\mu_o}\left[\sum_{n=0}^{\infty} k_{yn} A_n \cos\left(\frac{n\pi x}{a}\right) \sin(k_{yn} y) + \sum_{n=0}^{\infty}\left(\frac{n\pi}{b}\right) B_n \sin\left(\frac{n\pi y}{b}\right) \cos(k_{xn} x)\right] , \tag{14}$$

$$H_{3y} = \frac{-1}{i\omega\mu_o}\left[\sum_{n=0}^{\infty}\left(\frac{n\pi}{a}\right) A_n \sin\left(\frac{n\pi x}{a}\right) \cos(k_{yn} y) + \sum_{n=0}^{\infty} k_{xn} B_n \cos\left(\frac{n\pi y}{b}\right) \sin(k_{xn} x)\right] , \tag{15}$$

where

$$k_{yn} = \left[k^2 - \left(\frac{n\pi}{a}\right)^2\right]^{1/2} , \tag{16}$$

$$k_{xn} = \left[k^2 - \left(\frac{n\pi}{b}\right)^2\right]^{1/2} , \tag{17}$$

and A_n and B_n are unknown coefficients.

Note that each term in (13) - (15) satisfies the scalar wave equation. Also, the A_n coefficients can be determined from H_{3x} at $y = b$, and the B_n coefficients can be determined from H_{3y} at $x = a$.

BOUNDARY CONDITIONS

The boundary conditions are that the tangential electric and magnetic fields are continuous at the interfaces between the cavity region and the waveguide regions:

$$(H_{1x} - H_{3x})\Big|_{y=b} = 0 \ , \tag{18}$$

$$(H_{2y} - H_{3y})\Big|_{x=a} = 0 \ , \tag{19}$$

$$(E_{1z} - E_{3z})\Big|_{y=b} = 0 \ , \tag{20}$$

$$(E_{2z} - E_{3z})\Big|_{x=a} = 0 \ . \tag{21}$$

By substituting the field expansions into (18) - (21), we obtain the following

$$kS_m \cos(k\hat{C}_m x)\sin(kS_m b) + \sum_{n=1}^{\infty} ikS_n R_{n,m} \cos(kC_n x)\exp(-ikS_n b)$$
$$- \sum_{n=0}^{\infty} k_{yn} A_n \cos\left(\frac{n\pi x}{a}\right) \sin(k_{yn} b) = 0 \tag{22}$$

$$ik \sum_{n=1}^{\infty} \hat{S}_n Q_{n,m} \cos(kC_n y)\exp(-ik\hat{S}_n a) + \sum_{n=0}^{\infty} k_{xn} B_n \cos\left(\frac{n\pi y}{b}\right) \sin(k_{xn} a) = 0 \tag{23}$$

$$\cos(kC_m x)\cos(kS_m b) + \sum_{n=1}^{\infty} R_{n,m} \cos(kC_n x)\exp(-ikS_n b)$$
$$- \sum_{n=0}^{\infty} A_n \cos\left(\frac{n\pi x}{a}\right) \cos(k_{yn} b) - \sum_{n=0}^{\infty} B_n \cos(n\pi)\cos(k_{xn} x) = 0 \tag{24}$$

$$\sum_{n=1}^{\infty} Q_{n,m} \cos(k\hat{C}_n y)\exp(-ik\hat{S}_n a) - \sum_{n=0}^{\infty} A_n \cos(n\pi)\cos(k_{yn} y)$$
$$- \sum_{n=0}^{\infty} B_n \cos\left(\frac{n\pi y}{b}\right) \cos(k_{xn} a) = 0 \tag{25}$$

Although (22) - (25) represent four equations in four sets of unknowns, we can solve for A_n in terms of $R_{n,m}$ in (22) and for B_n in terms of $Q_{n,m}$ in (23). If we multiply (22) by $\cos(p\pi x/a)$ and integrate on x from 0 to a, we obtain

$$A_p = G_{p,m} + \sum_{n=0}^{\infty} F_{n,p} R_{n,m} \ , \tag{26}$$

where

$$G_{p,m} = \frac{\varepsilon_p kS_m \sin(kS_m b) I_{pm}}{k_{yp} a \sin(k_{yp} b)} \ , \tag{27}$$

$$F_{n,p} = \frac{ikS_n\varepsilon_p I_{pn}\exp(-ikS_n b)}{k_{yp}a\,\sin(k_{yp}b)}\,, \tag{28}$$

$$I_{pn} = \frac{a}{2}\left[\frac{\sin(p\pi - kC_n a)}{(p\pi - kC_n a)} + \frac{\sin(p\pi + kC_n a)}{(p\pi + kC_n a)}\right], \tag{29}$$

and

$$\varepsilon_p = \begin{cases} 1, & p = 0 \\ 2, & p \neq 0 \end{cases} \tag{30}$$

Similarly, if we multiply (23) by $\cos(p\pi y/b)$ and integrate on y from 0 to b, we obtain

$$B_p = \sum_{n=0}^{\infty} \hat{F}_{n,p} Q_{n,m}\,, \tag{31}$$

where

$$\hat{F}_{n,p} = \frac{ik\hat{S}_n\varepsilon_p\hat{I}_{pn}\exp(-ik\hat{S}_n a)}{k_{xp}b\,\sin(k_{xp}a)}\,, \tag{32}$$

and

$$\hat{I}_{pn} = \frac{b}{2}\left[\frac{\sin(p\pi - k\hat{C}_n b)}{(p\pi - k\hat{C}_n b)} + \frac{\sin(p\pi + k\hat{C}_n b)}{(p\pi + k\hat{C}_n b)}\right]. \tag{33}$$

Thus we can analytically eliminate the cavity coefficients, A_p and B_p, in terms of the desired waveguide coefficients, $R_{n,m}$ and $Q_{n,m}$.

MODE MATCHING

In order to derive a set of linear equations from (24), we multiply (24) by the waveguide mode field, $\cos(kC_p x)$, and integrate on x from 0 to a. Because of the orthogonality of the waveguide modes, only one term in the $R_{n,m}$ summation remains, and the result is

$$R_{p,m} = E_{p,m} + \sum_{n=0}^{\infty}[H_{n,p}A_n + L_{n,p}B_n]\,, \tag{34}$$

where

$$E_{p,m} = \frac{-\delta_{mp}\cos(kS_p b)}{\exp(-ikS_p b)}\,, \tag{35}$$

$$H_{n,p} = \frac{\cos(k_{yn}b)I_{np}}{N_p\exp(-ikS_p b)}\,, \tag{36}$$

$$L_{n,p} = \frac{(-1)^n J_{np}}{N_p\exp(-ikS_p b)}\,, \tag{37}$$

$$N_p = \frac{a}{2}\left[1 + \frac{\sin(2kC_p a)}{2kC_p a}\right], \tag{38}$$

$$J_{np} = \frac{a}{2}\left[\frac{\sin(k_{xn}a - kC_p a)}{(k_{xn}a - kC_p a)} + \frac{\sin(k_{xn}a + kC_p a)}{(k_{xn}a + kC_p a)}\right], \tag{39}$$

and

$$\delta_{mp} = \begin{cases} 1, & m = p \\ 0, & m \neq p \end{cases} \tag{40}$$

In a similar manner, we multiply (25) by the waveguide mode field, $\cos(k\hat{C}_p y)$, and integrate on y from 0 to b to obtain

$$Q_{p,m} = \sum_{n=0}^{\infty} (\hat{H}_{np} A_n + \hat{L}_{np} B_n) , \tag{41}$$

where

$$\hat{H}_{np} = \frac{(-1)^n \hat{J}_{np}}{\hat{N}_p \exp(-ik\hat{S}_p a)} , \tag{42}$$

$$\hat{L}_{np} = \frac{\cos(k_{xn}a) I_{np}}{\hat{N}_p \exp(-ik\hat{S}_p a)} , \tag{43}$$

and

$$\hat{N}_p = \frac{b}{2}\left[1 + \frac{\sin(2k\hat{C}_p b)}{2k\hat{C}_p b}\right], \tag{44}$$

and

$$\hat{J}_{np} = \frac{b}{2}\left[\frac{\sin(k_{yn}b - k\hat{C}_p b)}{(k_{yn}b - k\hat{C}_p b)} + \frac{\sin(k_{yn}b + k\hat{C}_p b)}{(k_{yn}b - k\hat{C}_p b)}\right], \tag{45}$$

In order to obtain two sets of equations for the two sets of waveguide coefficients, $R_{p,m}$ and $Q_{p,m}$ we substitute (26) and (31) into (34) and (41) with the following result

$$R_{p,m} - \sum_{q=1}^{\infty}\left[\sum_{n=0}^{\infty} F_{qn}H_{np}\right]R_{q,m} - \sum_{q=1}^{\infty}\left[\sum_{n=0}^{\infty} F_{qn}L_{np}\right]Q_{q,m} = E_{pm} + \sum_{n=0}^{\infty} H_{np}G_{nm} , \tag{46}$$

and

$$Q_{p,m} - \sum_{q=1}^{\infty}\left[\sum_{n=0}^{\infty} \hat{F}_{qn}\hat{L}_{np}\right]Q_{q,m} - \sum_{q=1}^{\infty}\left[\sum_{n=0}^{\infty} F_{qn}\hat{H}_{np}\right]R_{q,m} = \sum_{n=0}^{\infty} \hat{H}_{np}G_{nm} . \tag{47}$$

A doubly infinite set of equations is obtained by letting p take on integer values from 1 to ∞ in (46) and (47). In order to solve the system, we retain only a finite number P_R of $R_{p,m}$ coefficients and a finite number P_Q of $Q_{p,m}$ coefficients. This results in the following matrix form

$$\begin{bmatrix} P_R + P_Q \\ \\ \text{by} \\ \\ P_R + P_Q \end{bmatrix} \begin{bmatrix} R_{1,m} \\ \vdots \\ R_{P_R,m} \\ Q_{1,m} \\ \vdots \\ Q_{P_Q,m} \end{bmatrix} = \begin{bmatrix} P_Q + P_R \\ \\ \text{by} \\ \\ 1 \end{bmatrix} \tag{48}$$

The matrix in (48) can be inverted to solve for the $R_{n,m}$ and $Q_{n,m}$ values. If in turn the incident mode number m is varied, the $R_{n,m}$ and $Q_{n,m}$ values essentially define a scattering matrix for a two-port waveguide junction. [Kerns and Beatty, 1967]. The cavity mode coefficients, A_n and B_n, were eliminated analytically to reduce the number of unknowns. Generally the cavity fields are of little interest, but if desired, A_n and B_n could be computed from (26) and (31).

NUMBERICAL RESULTS

In this section we present numerical results for frequencies from 50 MHz to 200 MHz. In all cases we take $a = b = 2m$ and also $Z_a = Z_b$. For the wall impedances, we use the following expression [Mahmoud and Wait, 1974]:

$$Z_a = Z_b = \left[\frac{\mu_o}{\varepsilon - \varepsilon_o - i\sigma/\omega}\right]^{1/2} \tag{49}$$

where ε and σ are the rock permittivity and conductivity. Here we treat both the case of perfectly conducting walls ($Z_a = Z_b = 0$) and imperfect walls ($\varepsilon/\varepsilon_o = 10$ and $\sigma = 10^{-2}$ mho/m).

Before presenting the corner results, we show the attenuation rates of the lowest order modes for the straight guide as obtained from (A-8) in Fig. 3. For perfectly conducting walls, the cutoff frequencies are 37.5 MHz for mode 1, 112.5 MHz for mode 2, and 187.5 MHz for mode 3. As shown in Fig. 3, the finite wall conductivity produces attenuation above cut off and smooths out the transition near cut off. However, in either case the attenuation rate is very high

below cutoff. Thus we show only results for the first three modes in the following curves.

A computer program was written for the matrix solution of (48). The perfectly conducting case ($Z_a = Z_b = 0$) was first examined because the checks on power conservation, reciprocity, and the edge condition are most easily performed for perfectly conducting walls. The convergence of the magnitude and phase of $R_{1,1}$ and $Q_{1,1}$ is shown in Figs. 4 and 5. In general it was found that convergence was reached with about twelve modes for any frequency below 200 MHz. Conservation of power as discussed in Appendix B was typically satisfied with a relative error of less than 10^{-6}. A further check, using the edge condition as discussed in Appendix D, revealed that both $Q_{n,m}$ and $R_{n,m}$ have the proper asymptotic behavior for large n.

In Figs. 6 and 7, the magnitudes of the Q's and R's are shown from 50 MHz to 200 MHz for perfectly conducting walls. The values of $|Q_{1,1}|$, $|Q_{2,1}|$, and $|Q_{3,1}|$ are representative of the strengths of the three modes transmitted into the side tunnel for the lowest order mode 1 incident. The phases are also available, but are of less interest. Similarly the R values represent the three reflected mode amplitudes for the lowest order mode incident. Both the Q's and R's are only shown above their cutoff frequencies where the modes are propagating. The amplitudes of the higher order evanescent modes are also available, but they are of little interest. The results in Figs. 6 and 7 show rapid variation near the cutoff frequencies, but the power conservation and edge condition checks are still well satisfied at all frequencies.

An additional check of reciprocity is also available for the results of Figs. 6 and 7 by letting mode 2 or 3 be the incident mode. From the results in Appendix C, the following reciprocal relations must hold

$$R_{2,1}\, S_2 = R_{1,2}\, S_1 \,, \quad Q_{2,1}\, S_2 = Q_{1,2}\, S_1$$

$$R_{3,1}\, S_3 = R_{1,3}\, S_1 \,, \quad Q_{3,1}\, S_3 = Q_{1,3}\, S_1 \qquad (50)$$

and

$$R_{3,2}\, S_3 = R_{2,3}\, S_2 \,, \quad Q_{3,2}\, S_3 = Q_{2,3}\, S_2$$

All the above relationships were found to be satisfied to five figures in both amplitude and phase. The reciprocity condition has been noted as a particularly useful test in rough surface scattering [Whitman and Schwering, 1979] because it checks both amplitude and phase.

In Figs. 8 and 9, analogous results are shown for imperfect walls. The results are similar to those in Figs. 6 and 7, but the sharp resonant peaks are reduced. Again the mode quantities, which are always finite, are shown only above cutoff. An interesting feature of the transmission ($Q_{n,m}$) amplitudes is that the higher order modes are more strongly excited than the lowest order mode for the lowest order mode incident. By reciprocity we could also expect the higher order modes to be more efficient in exciting the lowest order mode in the crosscut tunnel. This behavior is qualitatively consistent with the "diffuse" mode treatment of Emslie, Lagace and Strong [1975].

CONCLUDING REMARKS

The model of intersecting tunnels with imperfectly conducting walls has been analyzed by a three-region mode matching technique. The numerical solution is found to converge smoothly, and checks on power conservation, reciprocity, and the edge condition are well satisfied.

The frequency dependence of both the reflected and transmitted modes shows rapid variation near the cutoff frequencies. A general result is that the lowest order mode incident on the intersection is more efficient in exciting the higher order modes in the cross cut. By reciprocity, higher order modes are also more efficient in exciting the lowest order mode (which is the mode

of lowest attenuation) in the cross cut. Those same general remarks would apply to the case of odd mode excitation that needs to be done explicitly for a general study of the problem.

A worthwhile extension would be to treat a more general tunnel model with finitely conducting top and bottom walls. Also, both horizontal and vertical polarization should be considered, including the numerous hybrid modes that would be needed in a general formulation. Here one can still exploit the inherent symmetry properties of the waveguide junction and suitably superimpose even and odd excitations.

The effect of tunnel non-uniformities on mode conversion between the higher order and lowest order mode could be important in a realistic communication environment. We have not considered that aspect here. For example, energy in a low order mode in the main tunnel can be transferred to higher order modes via mode conversion when the tunnel walls are non-uniform. These converted higher order modes, in turn, would be transformed efficiently into low order modes in the cross tunnel regions. Thus a comprehensive analysis of the tunnel junction problem should incorporate all such refinements. What we have done here is to point the way for further work in the field.

APPENDIX A - MODAL EQUATION

The modal equation for the y-directed guide is obtained by substituting (2) and (5) into (7). Each mode must then satisfy the following

$$\cos(kC_n a) = \frac{kC_n Z_a}{i\omega\mu_o} \sin(kC_n a) \ . \qquad \text{(A-1)}$$

By replacing the cos and sin terms in (A-1) by their exponential forms the following form is obtained

$$\frac{C_n - 1/\Delta_a}{C_n + 1/\Delta_a} \exp(-i2kaC_n) - 1 = 0 \ , \qquad \text{(A-2)}$$

where $\Delta_a = Z_a/(\mu_o/\varepsilon_o)^{1/2}$. This form agrees with the more general modal equation for a parallel plate guide as given by Wait [1962].

An approximate solution for C_n can be obtained by making the following approximation

$$\frac{C_n - (1/\Delta_a)}{C_n + (1/\Delta_a)} \simeq -(1 - 2C_n\Delta_a) \simeq -\exp(-2C_n\Delta_a) \tag{A-3}$$

Thus, an approximate modal equation is

$$\exp[-C_n(2\Delta_a + 2ika)] = -1 = \exp[-i(2n - 1)\pi] \tag{A-4}$$

Now (A-4) is easily solved for C_n:

$$C_n \simeq \frac{(2n - 1)\pi}{2(ka - i\Delta_a)} \tag{A-5}$$

Actually (A-5) is exact for the case of a perfectly conducting wall ($\Delta_a = 0$). When Δ_a is not zero, we use (A-5) as a starting value for a numerical solution of (A-5) by Newton's method [Hamming, 1973].

For the x-directed guide, the situation is completely analogous, and the modal equation is

$$\frac{\hat{C}_n - (1/\Delta_b)}{\hat{C}_n + (1/\Delta_b)} \exp(-i2kb\hat{C}_n) - 1 = 0 \ , \tag{A-6}$$

where

$$\Delta_b = Z_b/(\mu_o/\varepsilon_o)^{1/2} \ . \tag{A-7}$$

The approximate solution is

$$\hat{C}_n \simeq \frac{(2n - 1)\pi}{2(kb - i\Delta_b)} \tag{A-8}$$

The attenuation rate α_n for the y-directed guide is simply given by

$$\alpha_n = -k\mathrm{Im}(S_n) \ (\text{nepers/m}) = -8.686k\mathrm{Im}(S_n) \ (\text{dB/m}) \ , \tag{A-9}$$

where $S_n = (1 - C_n^2)^{1/2}$.

APPENDIX B - POWER CONSERVATION

We restrict the derivation to the case of perfectly conducting walls ($\Delta_a = \Delta_b = 0$) where the waveguide modes have conjugate orthogonality and carry power independently. In order to simplify the calculation, we first rewrite the incident fields in (2) and (4) in terms of incoming and outgoing waves:

$$E_{1z} = \frac{1}{2}\left(\exp(+ikS_m y) + \exp(-ikS_m y)\right)\cos(kC_m x) + \sum_{n=1}^{\infty} R_{n,m}\cos(kC_n x)\exp(-ikS_n y) \tag{B-1}$$

and

$$H_{1x} = \frac{k}{i\omega\mu_o}\left[\frac{S_m}{2i}\left(\exp(ikS_m y) - \exp(-ikS_m y)\right)\cos(kC_m x) + \sum_{n=1}^{\infty} iS_n R_{n,m}\cos(kS_n x)\exp(-ikS_n y)\right] \tag{B-2}$$

The power into the cavity region 3, P_{in}, is due only to the incoming term (positive exponential):

$$P_{in} = \frac{1}{8}\frac{S_m}{(\mu_o/\varepsilon_o)^{1/2}}\int_o^a \cos^2(kC_m x)dx = \frac{S_m a}{16(\mu_o/\varepsilon_o)^{1/2}}. \tag{B-3}$$

The power out of the cavity region into region 1, P_{1out}, is due to the outgoing portion of the incident field plus all of the outgoing reflected fields:

$$P_{1out} = \frac{1}{2(\mu_o/\varepsilon_o)^{1/2}}\sum_{n=0}^{\infty}\mathrm{Re}(S_n)\left|R_{n,m} + \frac{1}{2}\delta_{n,m}\right|^2 \cdot \int_o^a \cos^2(kC_n x)dx \tag{B-4}$$

$$= \frac{a}{4(\mu_o/\varepsilon_o)^{1/2}}\sum_{n=0}^{\infty}\mathrm{Re}(S_n)\left|R_{n,m} + \frac{1}{2}\delta_{nm}\right|^2.$$

Note that the modes which are "cut off" have $\mathrm{Re}(S_n) = 0$ and will not contribute to the power.

The power out of the cavity into region 2, P_{2out}, is given by

$$P_{2out} = \frac{1}{2(\mu_o/\varepsilon_o)^{1/2}} \sum_{n=0}^{\infty} \mathrm{Re}(\hat{S}_n) |Q_{n,m}|^2 \cdot \int_o^b \cos^2(k\hat{C}_n y)\,dy$$

$$= \frac{b}{4(\mu_o/\varepsilon_o)^{1/2}} \sum_{n=0}^{\infty} \mathrm{Re}(\hat{S}_n) |Q_{n,m}|^2 \,. \tag{B-5}$$

Since the cavity region is lossless, the power in must equal the total power out:

$$P_{in} = P_{1out} + P_{2out} \,. \tag{B-6}$$

A measure of the relative power error in the numerical solution, E_p, is given by

$$E_p = \frac{P_{in} - P_{1out} + P_{2out}}{P_{in}} \,. \tag{B-7}$$

APPENDIX C

Here we treat only the propagating modes for perfectly conducting walls ($\Delta_a = \Delta_b = 0$). Thus S_n and $\hat{S}_m$ are real. An extensive treatment of the reciprocity relations for the scattering matrix has been given by Kerns and Beatty [1967]. However, for our two-port geometry, the reciprocity relationship for the reflected modes is simply

$$R_{n,m}S_n = R_{m,n}S_m \,. \tag{C-1}$$

The S_n and S_m factors arise from the fact that the power carried by the n^{th} mode is proportional to S_n [Kerns and Beatty, 1967].

In general, we would need to switch the input field to the x-directed guide in order to check $Q_{n,m}$. However, for the special case of $a = b$, we can derive the following by reciprocity and symmetry:

$$Q_{n,m}\hat{S}_n = Q_{m,n}\hat{S}_m \,. \tag{C-2}$$

Note that (C-1) and (C-2) are completely analogous to the reciprocity relations for plane wave scattering by periodic surfaces [Whitman and Schwering, 1979]. These relations are useful for supplementing the power conservation check because both amplitude and phase are involved.

APPENDIX D - EDGE CONDITION

Again we consider only the case of perfectly conducting walls ($\Delta_a = \Delta_b = 0$). In this case the edge condition is particularly simple [Mittra and Lee, 1971; Meixner, 1972]. The electric field varies as the distance from the edge to the two thirds power, and the radial magnetic field varies as the distance to the minus one third power. These relationships yield the following proportionalities for the waveguide fields near the corner:

$$E_{1z}\Big|_{y=b} \propto (a - x)^{2/3} , \tag{D-1}$$

$$E_{2z}\Big|_{x=a} \propto (b - y)^{2/3} , \tag{D-2}$$

$$H_{1x}\Big|_{y=b} \propto (a - x)^{-1/3} \tag{D-3}$$

$$H_{2y}\Big|_{x=a} \propto (b - y)^{-1/3} \tag{D-4}$$

The modal coefficients, $R_{n,m}$ for E_{1z} in (2) and $Q_{n,m}$ for E_{2z} in (8), must vary as $n^{-5/3}$ for large n in order to satisfy (D-1) and (D-2). Thus, from (2) and (8), we have the following proportionalities for large n:

$$R_{n,m} \propto n^{-5/3} \exp(ikbS_n) \tag{D-5}$$

and

$$Q_{n,m} \propto n^{-5/3} \exp(ika\hat{S}_n) \tag{D-6}$$

This behavior for large n comes naturally out of the solution, but in some modal treatments the asymptotic behavior has been built into the solution in order to speed convergence [Zaki and Neurenther, 1968; Howard, 1972; Hill and Wait, 1976].

REFERENCES

Copplestone, R.J., (1969), An exact three-dimensional field theory for a class of cyclic H-plane waveguide junction, *IEEE Trans. Microwave Theory Tech.*, MTT-27(6), 577-584.

Emslie, A.G., R.L. Lagace, and P.F. Strong, (1975), Theory of the propagation of UHF radio waves in coal mine tunnels, *IEEE Trans. Ant. Prop.*, AP-23(2), 192-205.

Hamming, R.W., (1973), *Numerical Methods for Scientists and Engineers*, McGraw-Hill, New York.

Hill, D.A. and J.R. Wait, (1976), Electromagnetic scattering of an arbitrary plane wave by a wire mesh with bonded junctions, *Can. J. Phys.*, 54, 354-361.

Howard, A.Q., (1972), On the mathematical theory of electromagnetic radiation from flanged waveguides, *J. Math. Phys.*, 13, 482-490.

Kerns, D.W. and R.W. Beatty, (1967), *Basic Theory of Waveguide Junctions*, Pergamon Press, New York.

Lewin, L., (1970), On the inadequacy of discrete mode-matching techniques in some waveguide discontinuity problems, *IEEE Trans. Microwave Theory Tech.*, MTT-18, (7), 364-372.

Mahmoud, S.F. and J.R. Wait, (1974), Geometrical optical approach for electromagnetic wave propagation in rectangular mine tunnels, *Radio Sci.*, 9(12), 1147-1158.

Morse, P.M. and H. Feshback, (1953), *Methods of Theoretical Physics*, 1368, McGraw-Hill, New York.

Murphy, J.N. and H.E. Parkinson, (1978), Underground mine communications, *Proc. IEEE*, 66(1), 26-50.

Meixner, J., (1972), The behavior of electromagnetic fields at edges, *IEEE Trans. Ant. Prop.*, AP-20(4), 442-446.

Mittra, R. and S.W. Lee, (1971), *Analytical Techniques in the Theory of Guided Waves*, Macmillan, New York.

Wait, J.R., (1962), *Electromagnetic Waves in Stratified Media*, Pergamon Press, New York [2nd Ed. 1970].

Whitman, R.J. and F. Schwering, (1979), Reciprocity identity for periodic surface scattering, *IEEE Trans. Ant. Prop.*, AP-27(2), 252-254.

Zaki, K.A. and A.R. Neureuther (1968), Numerical solutions of electromagnetic boundary value problems by means of the asymptotic anticipation method, *Radio Science*, 3(12), 1158-1167.

Acknowledgements

We wish to thank Ms. Jeri Bacon for help in preparing the manuscript, and Ms. Robin Healy for drafting the illustrations.

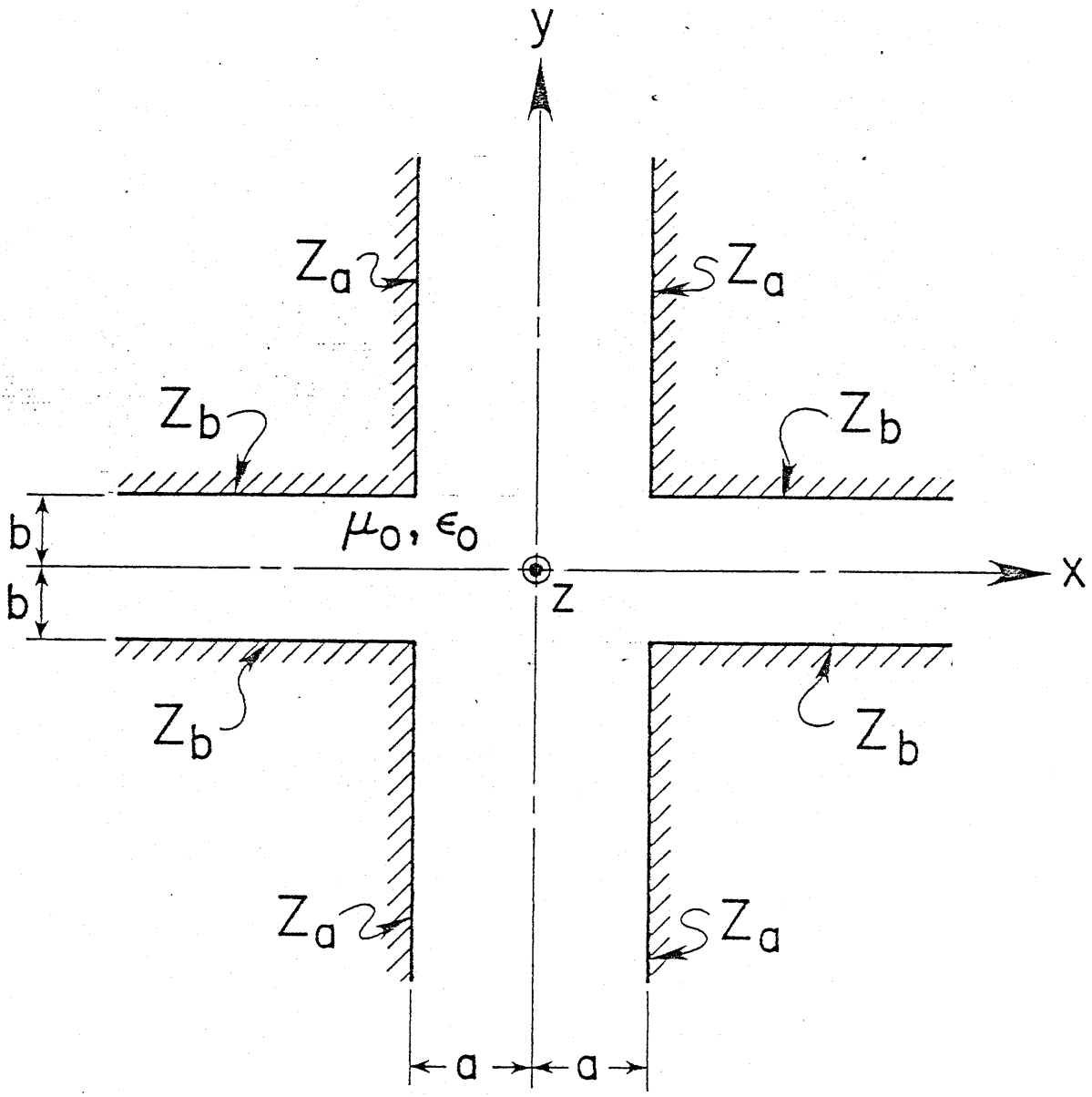

Figure 1. Right-angle intersection of tunnels with impedance walls.

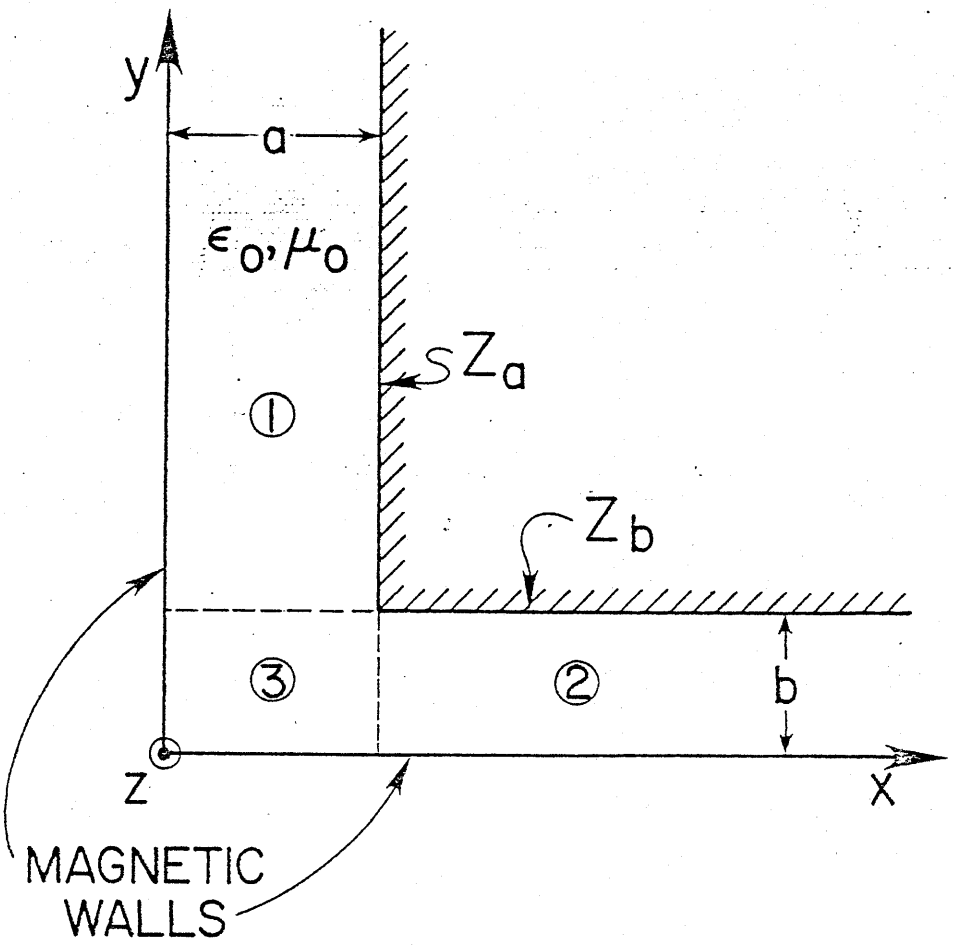

Figure 2. Equivalent geometry for even symmetry in x and y.

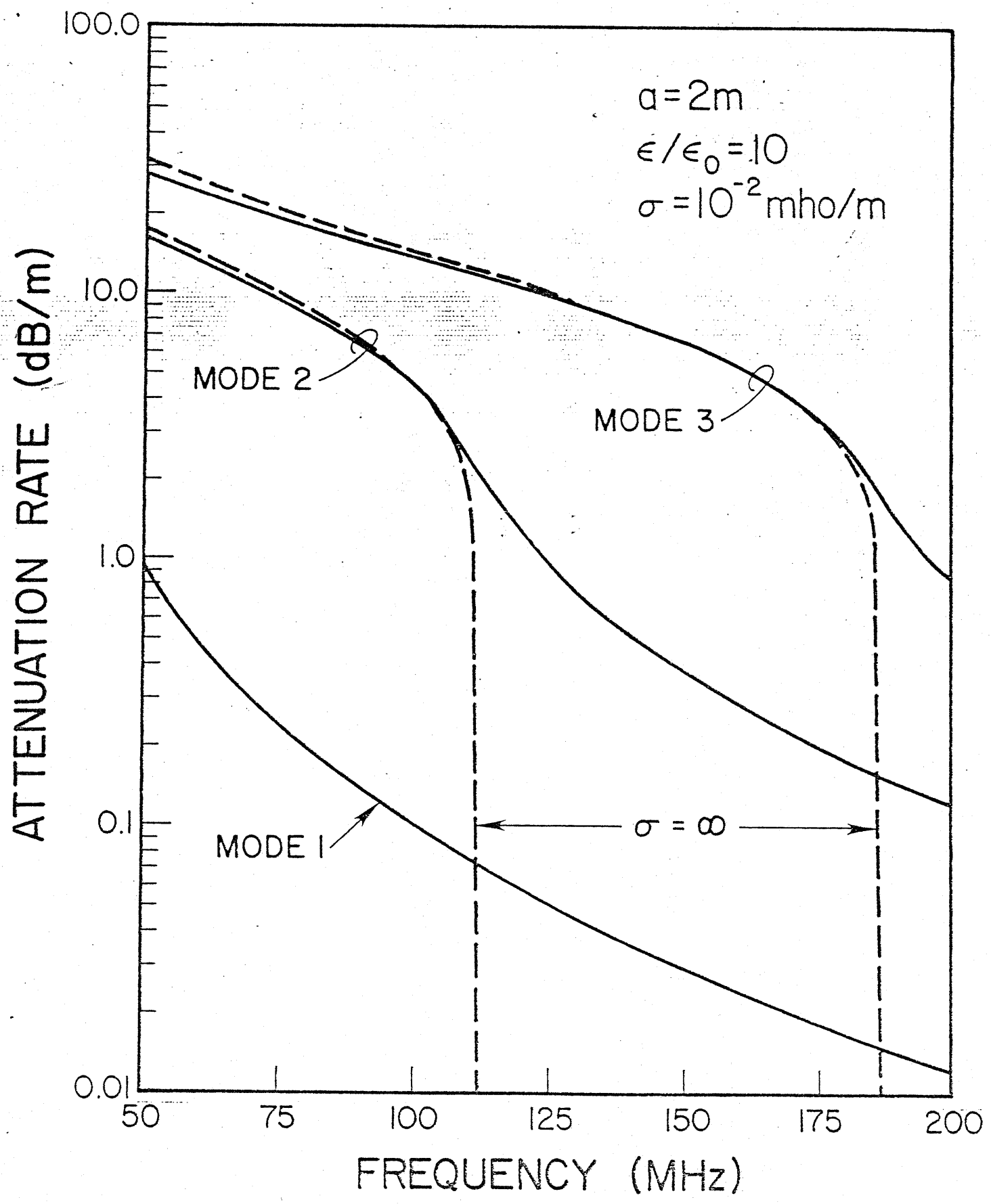

Figure 3. Attenuation rates of the lowest order modes for tunnel walls of finite and infinite conductivity.

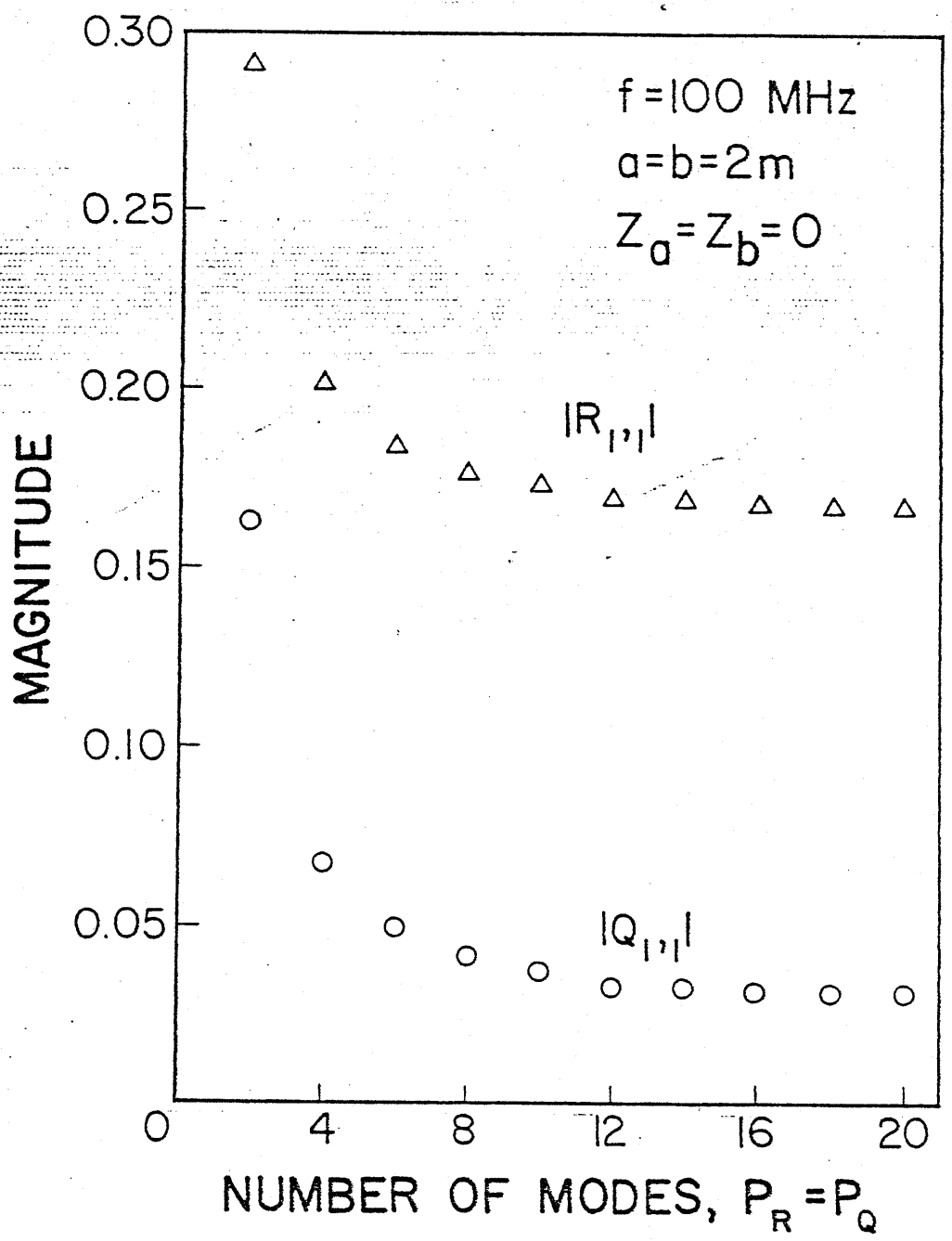

Figure 4. Convergence of the magnitudes of $R_{1,1}$ and $Q_{1,1}$ as the number of waveguide modes is increased.

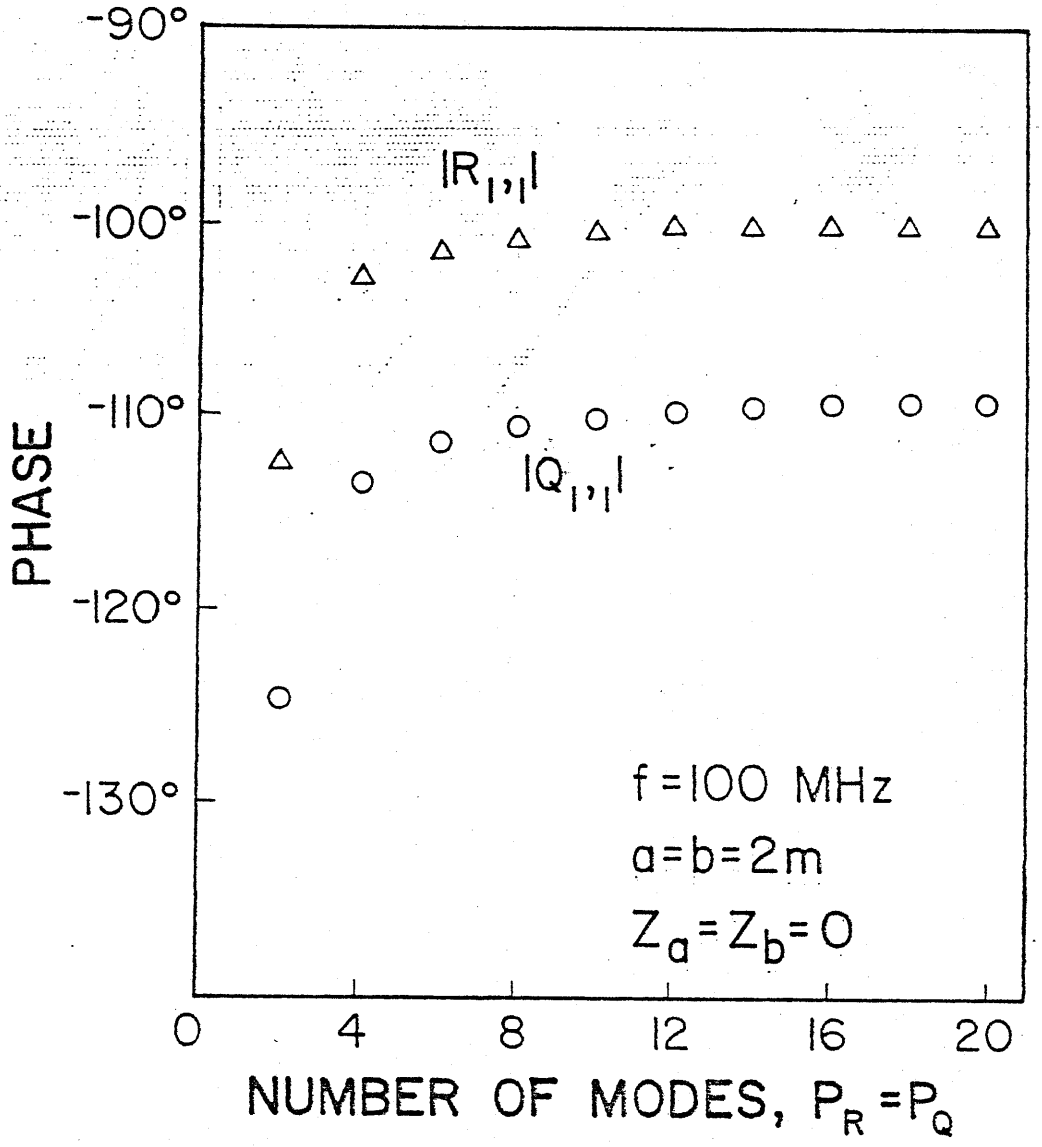

Figure 5. Convergence of the phases of $R_{1,1}$ and $Q_{1,1}$ as the number of waveguide modes is increased.

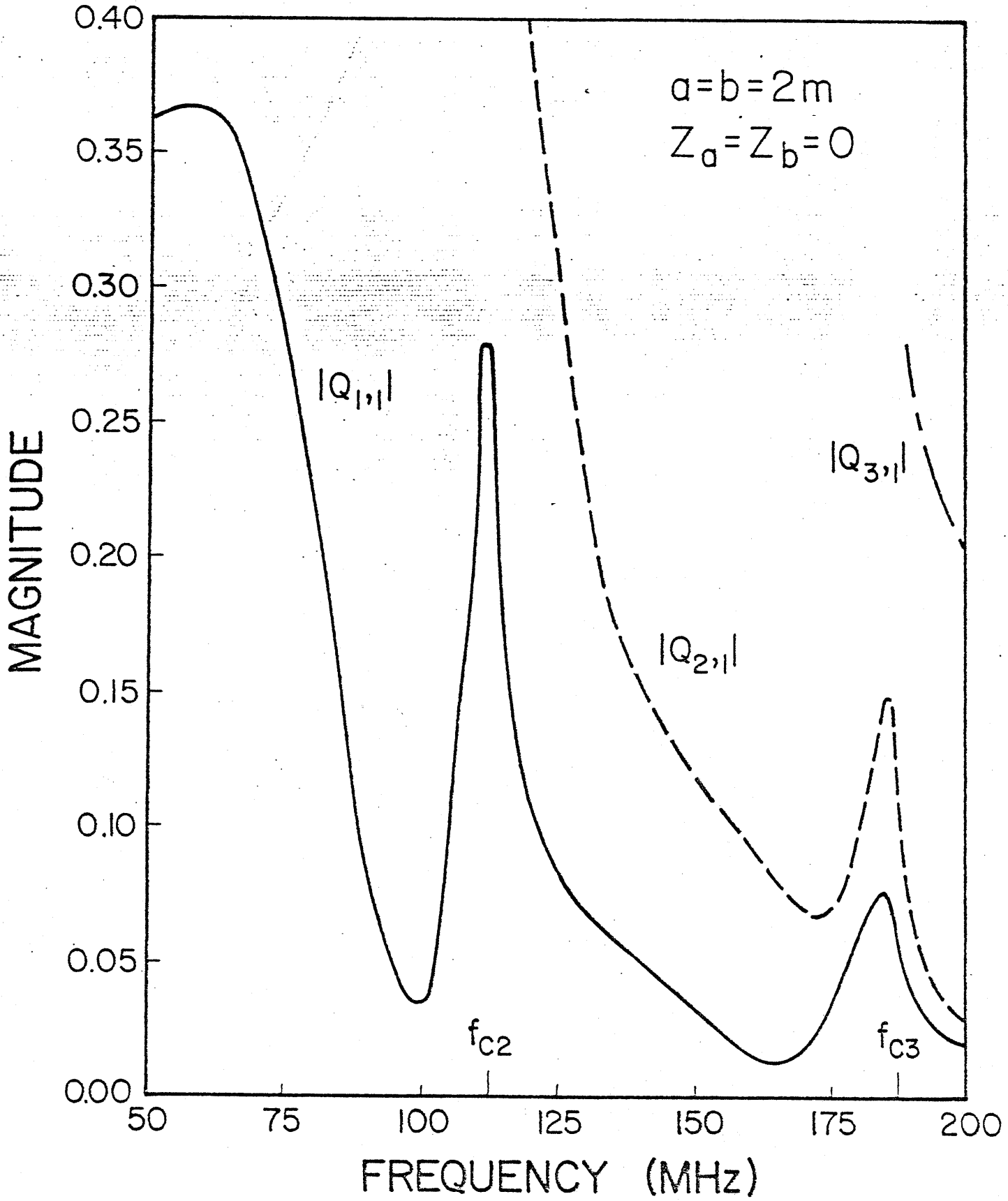

Figure 6. Magnitudes of the transmission coefficients for perfectly conducting walls.

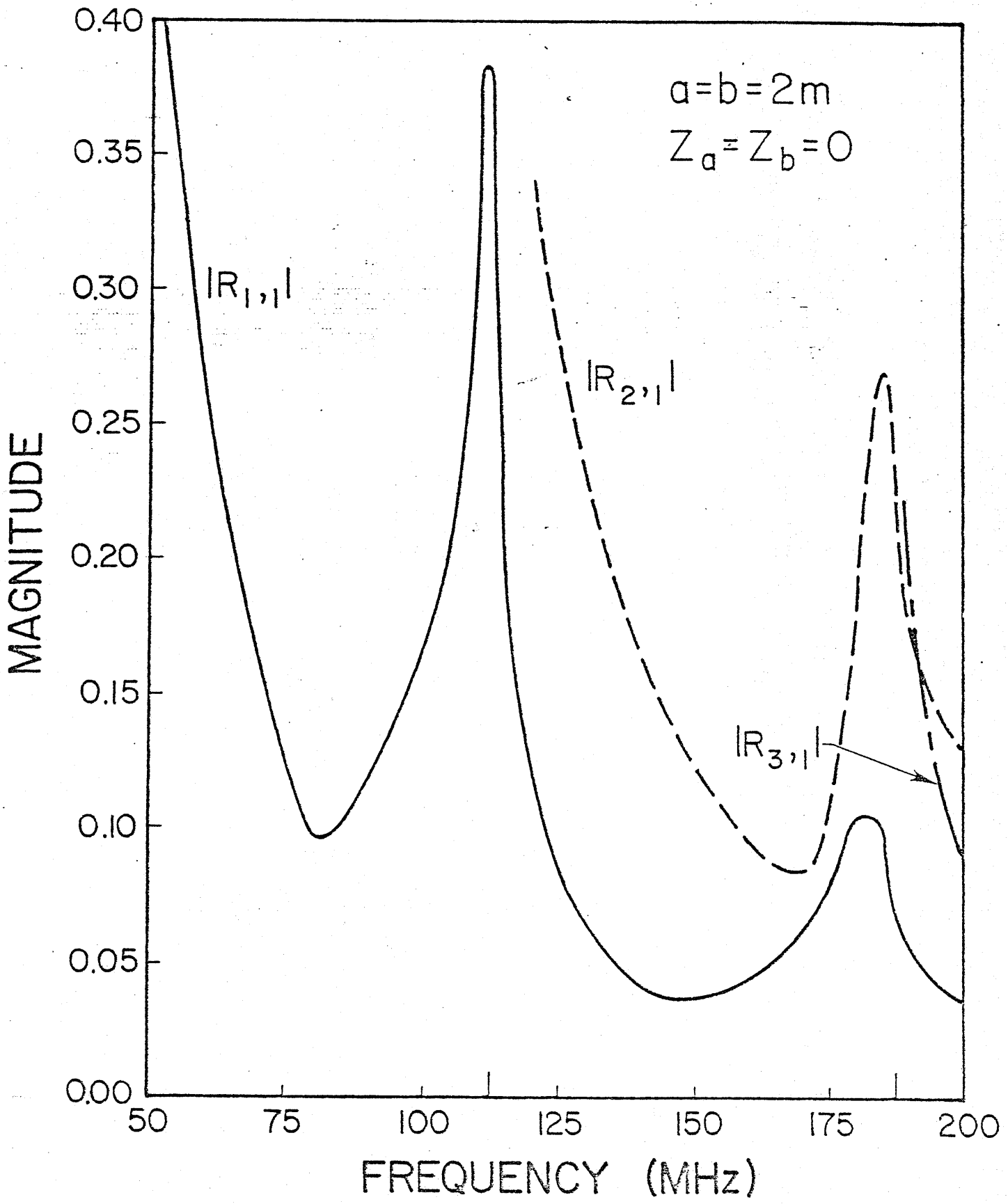

Figure 7. Magnitudes of the reflection coefficients for perfectly conducting walls.

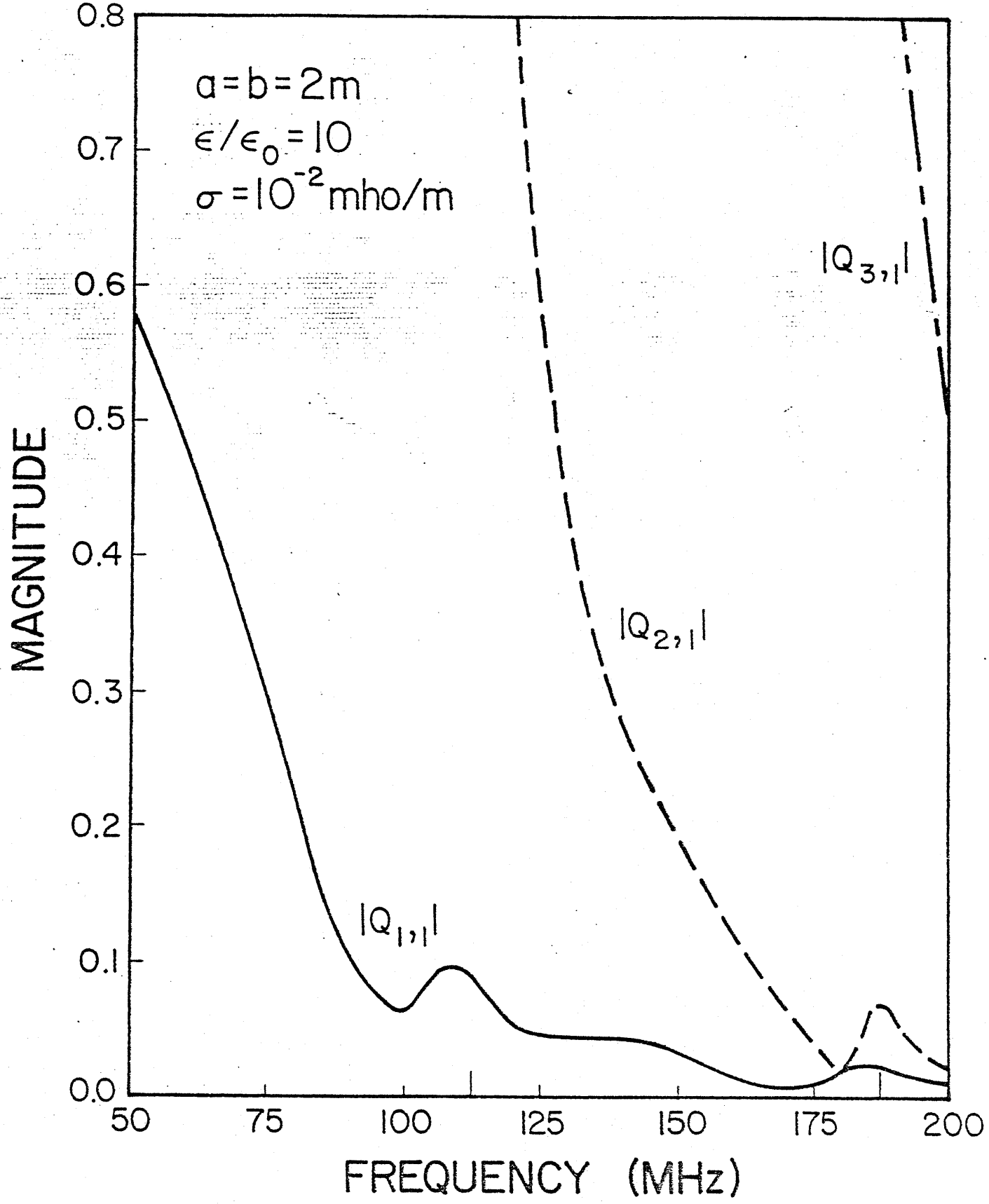

Figure 8. Magnitudes of the transmission coefficients for imperfectly conducting walls.

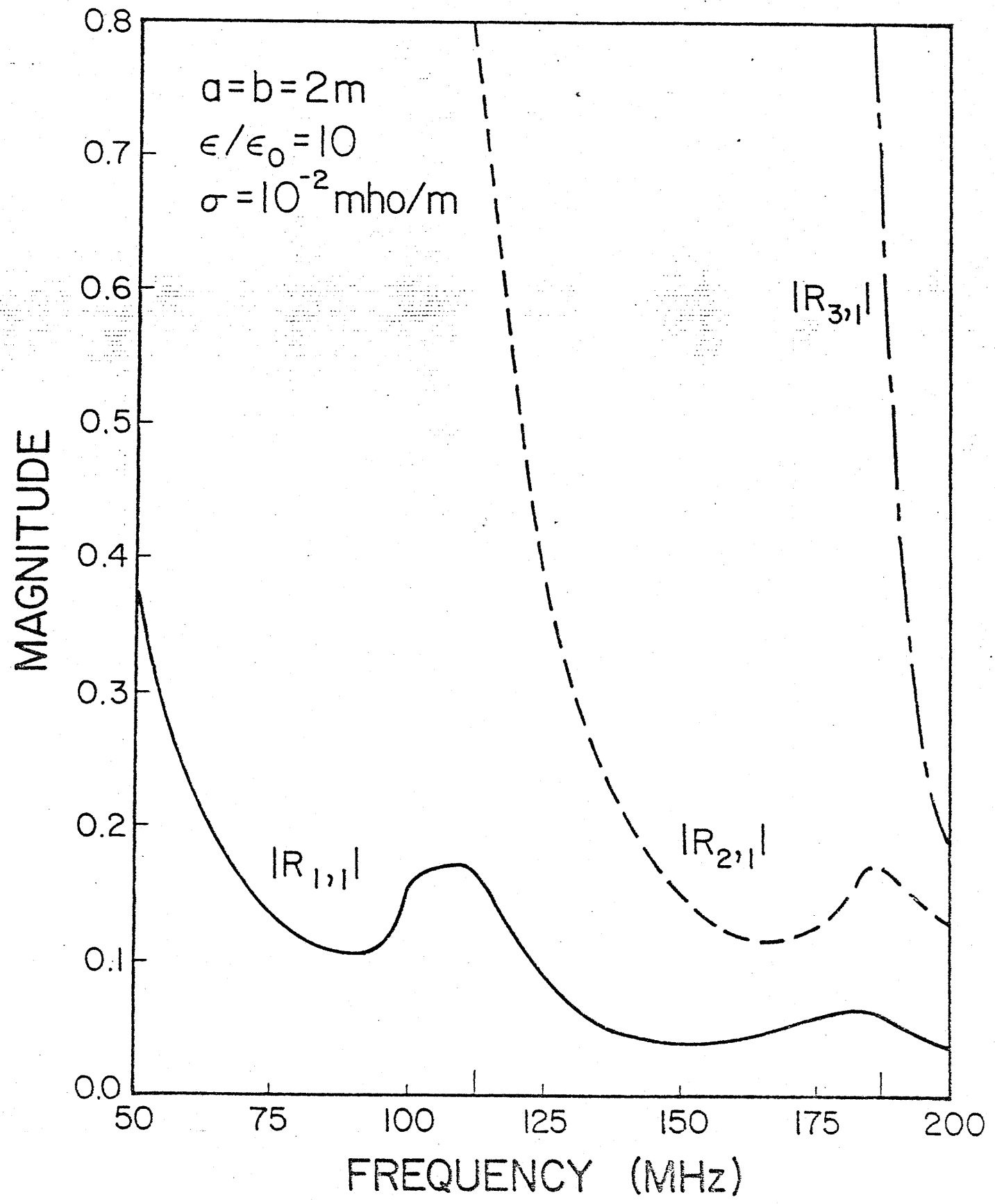

Figure 9. Magnitudes of the reflection coefficients for imperfectly conducting walls.

FIELDS OF A HORIZONTAL LOOP OF ARBITRARY SHAPE BURIED IN A TWO LAYER EARTH

by

JAMES R. WAIT and DAVID A. HILL
ERL/NOAA and ITS/NTIA
U.S. Department of Commerce
Boulder, Colorado 80309

Abstract - Expressions have been derived for the magnetic field in air produced by a buried horizontal loop of arbitrary shape. Numerical results are presented for both circular and rectangular loops. Rectangular loops produce an azimuthal magnetic field component which is not present in the case of a circular loop. The results have application to source location in mine rescue techniques. In such cases, frequencies in the audio range are employed and the assumption of a uniform current in the source loop is well justified.

INTRODUCTION

In communicating with and/or locating trapped miners, we had earlier suggested that a feasible source would be a wire loop that could be excited by a portable transmitter. A great deal of effort has gone into the problem by various groups in the U.S. and elsewhere. An accessible and very well written account can be found in the prize-winning paper by Large, Ball and Farstad [1973].

In a previous analysis, we considered the problem of a small horizontal loop or vertical magnetic dipole located in the bottom region of a two-layer earth. The results were quasi-static in the sense that all significant distances in the problem were small compared with a free space wavelength. Using numerical integration, the magnitude of the ratio of the horizontal to the vertical magnetic field was examined for an observer on the earth's surface. This

was shown to have diagnostic features that could be used as the basis of a source location technique, in spite of the fact that the curves were modified to some extent by the layer structure. [Wait, 1971; Wait and Spies, 1971a].

Here we extend the earlier analysis to allow for the finite extent of the source loop. Also, we derive explicit expressions for the fields that are valid everywhere. In order to render the problem some generality, displacement currents in the air and in the ground are retained at least in the initial formulation.

First of all we deal with a circular loop of radius a. When a tends to zero we then recover the field expressions given earlier for a magnetic dipole. We then consider a loop of finite size with any specified shape. In particular, we deal with one of rectangular form.

BASIC FORMULATION

The model for the circular loop is illustrated in Fig. 1. The earth is taken be a two layer structure where the upper layer or slab of thickness b is characterized by electrical properties σ_1, ε_1, and μ_1. The lower semi-infinite region corresponding properties σ_2, ε_2, and μ_2. With respect to a polar coordinate system (ρ,ϕ,z), the earth's surface is $z = 0$ and the lower interface of the upper slab is $z = -b$. The loop of radius a, carrying a total uniform current I, is located in the plane $z = -h$ and is coaxial with the z axis. The region $z > 0$ is assumed to be free space with electrical constants (ε_o, μ_o).

The source current and all associated electromagnetic fields are taken to vary as $\exp(i\omega t)$.

The source condition for the surface current density $j_\phi(\rho)$ in the plane $z = -h$ is given as follows

$$j_\phi(\rho) = I\delta(\rho - a) \tag{1}$$

where $\delta(\rho - a)$ is the unit impulse function. Here we find it convenient to apply the Fourier-Bessel transform in order to obtain the desired spectral form for the source field. Thus we have the pair

$$j_\phi(\rho) = \int_0^\infty f(\lambda) J_n(\lambda\rho)\lambda d\lambda \tag{2}$$

and

$$f(\lambda) = \int_{0^-}^\infty j_\phi(\rho) J_n(\lambda\rho)\rho d\rho \tag{3}$$

where n is an integer to be selected and J_n is a Bessel function of order n. Clearly, for the filamental current model,

$$f(\lambda) = IJ_n(\lambda a)a \tag{4}$$

By symmetry it is evident that the electromagnetic fields have only non-vanishing components E_ϕ, H_ρ and H_z. A subscript 1, 2, or 0 is added to these quantities when they refer specifically to the upper slab, lower region or free space respectively. In particular, we have the source conditions

$$H_{2\rho}(-h + 0) - H_{2\rho}(-h - 0) = j_\phi(\rho) \tag{5}$$

$$E_{2\phi}(-h + 0) - E_{2\phi}(-h - 0) = 0 \tag{6}$$

that must be met.

In view of the symmetry of the problem, it is apparent that the fields in any of the regions can be obtained from a magnetic Hertz vector that has only an axial component Π^* that we dub the "Hertz potential". Thus

$$E_\phi = i\mu\omega\partial\Pi^*/\partial\rho \tag{7}$$

$$H_\rho = \partial^2\Pi^*/\partial\rho\partial z \tag{8}$$

$$H_z = (-\gamma^2 + \partial^2/\partial z^2)\Pi^* \tag{9}$$

where

$$\gamma^2 = i\mu\omega(\sigma + i\varepsilon\omega).$$

Now because Π^* satisfies

$$\left(\frac{1}{\rho}\frac{\partial}{\partial\rho}\rho\frac{\partial}{\partial\rho} + \frac{\partial^2}{\partial z^2} - \gamma^2\right)\Pi^* = 0 \tag{10}$$

we easily deduce that solutions, finite at $\rho = 0$, have the form

$$\Pi^* = J_o(\lambda\rho)\exp(\mp uz) \tag{11}$$

where

$$u = (\lambda^2 + \gamma^2)^{1/2}.$$

Here λ is the transverse wave number than can be identified with the variable λ in equ. (2). In particular, we note that H_ρ is made up of linear combinations of solutions of the form $J_1(\lambda\rho)\exp(\mp uz)$ [on noting that $dJ_o(x)/dx = -J_1(x)$]. Now it is clearly evident we should choose $n = 1$ in (2), (3), and (4). Thus, our source current density, in the plane $z = -h$, should be given by

$$j_\phi(\rho) = Ia \int_o^\infty J_1(\lambda a)J_1(\lambda\rho)\lambda d\lambda \tag{12}$$

We are now in the position to write down the desired formsfor the Hertz potentials in the three regions:

$$\Pi_1^* = p \int_o^\infty A[e^{-u_1 z} + R_o e^{u_1 z}] \frac{J_1(\lambda a)}{u_2} J_o(\lambda\rho)d \tag{13}$$

$$\Pi_2^* = p \int_o^\infty [e^{-u_2|z+h|} + R_\perp e^{2u_2 b}\, e^{u_2(z-h)}] \frac{J_1(\lambda a)}{u_2} J_o(\lambda\rho)d\lambda \tag{14}$$

$$\Pi_o^* = p \int_o^\infty T_o e^{-u_o z} \frac{J_1(\lambda a)}{u_2} J_o(\lambda\rho)d\lambda \tag{15}$$

where the five functional coefficients p, A, R_o, $R_\perp$ and T_o are not yet known. Other multiplicative factors have been inserted to simplify the interpretation of the final results.

In order that (5) and (6) be satisfied, we readily deduce that $p = Ia/2$. The other four coefficients can be deduced by insisting that the tangential fields E_ϕ and H_ρ be continuous at the two interfaces $z = 0$ and $z = -b$. This algebraic process yields, for the reflection coefficients,

$$R_o = (N_1 - N_o)/(N_1 + N_o) \tag{16}$$

and

$$R_\perp = (N_2 - Y_1)/(N_2 + Y_1) \tag{17}$$

where $N_1 = u_1/i\mu_1\omega$, $N_2 = u_2/i\mu_2\omega$, $N_o = u_o/i\mu_o\omega$ and Y_1 are appropriate admittances. Here

$$Y_1 = -\left.\frac{H_{1\rho}}{E_{1\phi}}\right]_{z=-b} = N_1 \frac{1 - R_o e^{-2u_1 b}}{1 + R_o e^{-2u_1 b}} \tag{18}$$

Actually these results are immediately obvious if one bears in mind the transmission line analogy for such problems.

To relate A and T_o we write down the matching equations for continuity of H_ρ at $z = 0$ and $z = -b$:

$$u_1(1 - R_o)A = u_o T_o \tag{19}$$

$$u_1[e^{u_1 b} - R_o e^{-u_1 b}]A = u_2[e^{u_2 b} - R_\perp e^{u_2 b}]e^{-u_2 h} \tag{20}$$

Thus

$$T_o = \frac{u_2}{u_o}[(1 - R_o)(1 - R_\perp)e^{u_2 b}/(e^{u_1 b} - R_o e^{-u_1 b})]\, e^{-u_2 h} \tag{21}$$

and

$$A = [(u_2/u_1)(1 - R_\perp)e^{u_2 b}/(e^{u_1 b} - R_o e^{-u_1 b})]\, e^{-u_2 h} \tag{22}$$

which completes our task of finding the unknown coefficients.

Now using the identity

$$1 - R_\perp = 2Y_1/(N_2 + Y_1) \tag{23}$$

it is not difficult to show that

$$\frac{T_o}{u_2} = \frac{1}{u_o}\left(\frac{2N_o}{N_1 + N_o}\right)\left(\frac{2N_1}{N_2 + N_1}\right)[1 - R_o R_2 e^{-2u_1 b}]^{-1}\, e^{-u_2(h-b)}\, e^{-u_1 b} \tag{24}$$

where

$$R_2 = (N_1 - N_2)/(N_1 + N_2) \tag{25}$$

The right hand side of (24) can clearly be interpreted as the product of two transmission coefficients (in large parentheses) and a propagation factor $\exp[-u_2(h-b) - u_1 b]$ corresponding to the one way transmission loss from the source to the bottom of the upper slab and then through the slab to the surface. The bracketed factor, when expanded, can be interpreted as the effect of multiple reflections within the slab, e.g.,

$$[1 - R_o R_2 e^{-2u_1 b}]^{-1} = 1 + R_o R_2 e^{-2u_1 b} + (R_o R_2)^2 e^{-4u_1 b} + \ldots \tag{26}$$

The field quantities of special interest are the magnetic components $H_{o\rho}$ and H_{oz} in the free space region. These are obtained from

$$H_{o\rho} = \partial^2 \Pi_o^* / \partial\rho\partial z \tag{27}$$

and

$$H_{oz} = (-\gamma_o^2 + \partial^2/\partial z^2)\Pi_o^* \tag{28}$$

where $\gamma_o^2 = -\varepsilon_o \mu_o \omega^2$.

A special case of particular interest is when all distances are small compared with the free space wavelength. Thus, we can say that $|\gamma_o \ell| << 1$ where ℓ is a typical distance. This amounts to setting $\gamma_o = 0$ in the general formulae derived above. Furthermore, to simplify the discussion we set $\mu_1 = \mu_2 = \mu_o$ then, for example, $N_1/N_2 = u_1/u_2$ and $N_o/N_1 = u_o/u_1 = \lambda/u_1$.

Using the preceding simplifications, we find without difficulty that

$$T_o = \frac{u_2}{u_o} T = \frac{u_2}{\lambda} T \tag{29}$$

where

$$T = \frac{\left(\frac{2\lambda}{u_1 + \lambda}\right)\left(\frac{2u_1}{u_1 + u_2}\right) \exp[-u_2(h - b) - u_1 b]}{1 - \left(\frac{u_1 - \lambda}{u_1 + \lambda}\right)\left(\frac{u_1 - u_2}{u_1 + u_2}\right) \exp[-2u_1 b]} \tag{30}$$

where $u_1 = (\lambda^2 + \gamma_1^2)^{1/2}$ and $u_2 = (\lambda^2 + \gamma_2^2)^{1/2}$. The desired field components in the quasi-static approximation can be written

$$H_{o\rho} = b_o P \quad \text{and} \quad H_{oz} = b_o Q \tag{31}$$

where

$$b_o = I(\pi a^2)/(2\pi h^3)$$

$$P = \frac{h^3}{2} \int_o^\infty \lambda^2 T(\lambda) e^{-\lambda z} J_1(\lambda\rho) \frac{2J_1(\lambda a)}{\lambda a} d\lambda \tag{32}$$

and

$$Q = \frac{h^3}{2} \int_o^\infty \lambda^2 T(\lambda) e^{-\lambda z} J_o(\lambda\rho) \frac{2J_1(\lambda a)}{\lambda a} d\lambda \tag{33}$$

The limiting case of a magnetic dipole is obtained by letting a become vanishingly small whence $2J_1(\lambda a)/(\lambda a) \to 1$, in the above expressions. The generalization of (30) to a three-layered earth is indicated in the Appendix.

HORIZONTAL LOOP OF ANY SHAPE

It is actually a very simple matter to generalize the above results to a horizontal loop whose profile is non-circular. To this end we write down the Hertz potential $d^2\Pi_o^*$ in the free space region for a current loop of elemental area $dx'dy'$ located at $(x',y',-h)$ with reference to the cartesian system of coordinates (x,y,z). Thus,

$$d^2\Pi_o^* = \frac{I dx'dy'}{4\pi} \int_o^\infty T(\lambda) e^{-\lambda z} J_o\left(\lambda[(x - x') + (y - y')^2]^{1/2}\right) d\lambda$$

for the usual quasi-static approximation wherein $\gamma_o = 0$ and $u_o = \lambda$. Then, of course,

$$\Pi_o^* = \frac{IA}{4\pi} \int_o^\infty T(\lambda) e^{-\lambda z} f(\lambda) d\lambda \tag{35}$$

where

$$f(\lambda) = \frac{1}{A} \int_{\text{Area}} \int \left(J_o\, \lambda[(x - x')^2 + (y - y')^2]^{1/2}\right) dx'dy' \tag{36}$$

and A is the area of the loop.

The desired magnetic field components expressed in cartesian coordinates are now obtained from

$$H_{ox} = \partial^2\Pi_o^*/\partial x \partial z \tag{37}$$

$$H_{oy} = \partial^2\Pi_o^*/\partial y \partial z \tag{38}$$

and

$$H_{oz} = \partial^2\Pi_o^*/\partial z^2 \tag{39}$$

In carrying out these operations we note that

$$\partial J_o(\lambda\hat{\rho})/\partial x = -J_1(\lambda\hat{\rho})\lambda\partial\hat{\rho}/\partial x = -J_1(\lambda\hat{\rho})\lambda(x - x')/\hat{\rho}$$

where $\hat{\rho} = [(x - x')^2 + (y - y')^2]^{1/2}$. Then we may write

$$H_{ox} = b_o P_x \tag{40}$$

$$H_{oy} = b_o P_y \tag{41}$$

$$H_{oz} = b_o P_z \tag{42}$$

where

$$P_{\substack{x \\ y}} = \frac{h^3}{2}\int_o^\infty \lambda^2 T(\lambda) e^{-\lambda z} f_{\substack{x \\ y}}(\lambda) d\lambda \tag{43}$$

and

$$P_z = \frac{h^3}{2}\int_o^\infty \lambda^2 T(\lambda) e^{-\lambda z} f(\lambda) d\lambda \tag{44}$$

where $b_o = IA/(2\pi h^3)$

Here

$$f_x(\lambda) = \frac{1}{A}\iint_{\text{Area}} J_1(\lambda\hat{\rho})\,\frac{x - x'}{\hat{\rho}}\,dx'dy' \tag{45}$$

and

$$f_y(\lambda) = \frac{1}{A}\iint_{\text{Area}} J_1(\lambda\hat{\rho})\,\frac{y - y'}{\hat{\rho}}\,dx'dy' \tag{46}$$

and $f(\lambda)$ is given by (36). One may note that

$$f_x(\lambda) = -\lambda^{-1}\partial f(\lambda)/\partial x \tag{47}$$

and

$$f_y(\lambda) = -\lambda^{-1}\partial f(\lambda)/\partial y. \tag{48}$$

An approach to evaluate (36) is to introduce new variables (r,θ) defined by

$$x' - x = r\cos\theta$$

$$y' - y = r\sin\theta$$

The element of area then becomes $rdrd\theta$ and

$$f(\lambda) = \frac{1}{A}\int_o^{2\pi}\int_o^{r_o(\theta)} J_o(\lambda r)\,rdrd\theta \tag{49}$$

where $r = r_o(\theta)$ is the equation for the profile of the loop that is contained in the plane $z = -h$. Using the Bessel function identity

$$\int_0^{\alpha} J_o(\alpha)\alpha d\alpha = \alpha J_1(\alpha) \tag{50}$$

it follows that

$$f(\lambda) = \frac{1}{A\lambda} \int_o^{2\pi} J_1\big(\lambda r_o(\theta)\big) r_o(\theta) d\theta \tag{51}$$

Of course, if $r_o(\theta) = a$, we obtain

$$f(\lambda) = \frac{2}{\lambda a} J_1(\lambda a) \tag{52}$$

which is the expected value.

REDUCTION OF INTEGRALS

Strictly speaking, (39) to (51) are valid only when the projection of the observation point (x,y) in the plane of the loop ($z = -h$) lies inside the loop. When the observation point lies outside the loop, (49) becomes

$$f(\lambda) = \frac{1}{A} \int_{\theta_1}^{\theta_2} \int_{r_i(\theta)}^{r_o(\theta)} J_o(\lambda r) r dr d\theta \ , \tag{53}$$

where θ_1 and θ_2 are the tangent angles and r_i is the inner radius as shown in Figure 2. The r integration can again be performed analytically by use of (50):

$$f(\lambda) = \frac{1}{A\lambda} \int_{\theta_1}^{\theta_2} [J_1(\lambda r_o(\theta))\, r_o(\theta) - J_1(\lambda r_i(\theta))\, r_i(\theta)] d\theta \ . \tag{54}$$

When the projection of the observation point lies on the loop boundary, (51) and (54) are equivalent.

In order to evaluate $f_x(\lambda)$ and $f_y(\lambda)$, we utilize the following identities involving $\hat{\rho}$:

$$\frac{\partial \hat{\rho}}{\partial x} = - \frac{\partial \hat{\rho}}{\partial x'} \quad \text{and} \quad \frac{\partial \hat{\rho}}{\partial y} = - \frac{\partial \hat{\rho}}{\partial y'} \ . \tag{55}$$

Thus (47) can be written

$$f_x(\lambda) = \frac{1}{A\lambda} \iint_{\text{Area}} \frac{\partial}{\partial x'} J_o(\lambda \hat{\rho}) dx' dy' \ . \tag{56}$$

The x' integration can be performed analytically to yield

$$f_x(\lambda) = \frac{1}{A\lambda}\int_{y_1'}^{y_2'}[J_o(\lambda\hat{\rho})\Big|_{x'=x_2'(y)} - J_o(\lambda\hat{\rho})\Big|_{x'=x_1'(y)}]dy' , \qquad (57)$$

where y_2' and y_1' are the upper and lower limits of y' and x_2' and x_1' are the upper and lower limits of x' and are functions of y. In a completely analagous manner, $f_y(\lambda)$ can be written

$$f_y(\lambda) = \frac{1}{A\lambda}\int_{x_1'}^{x_2'}[J_o(\lambda\hat{\rho})\Big|_{y'=y_2'(x)} - J_o(\lambda\hat{\rho})\Big|_{y'=y_1'(x)}]dx' . \qquad (58)$$

Thus, $f(\lambda)$, $f_x(\lambda)$, and $f_y(\lambda)$ have all been reduced to a single integral.

RECTANGULAR LOOP

Another case of some interest is the rectangular loop, since this shape might be quite feasible for underground workings. Thus, for a rectangle with dimensions $2s$ by 2ℓ, the vertices in the plane $z = -h$ would be located at $(s,\ell,)$, $(-s,\ell)$, $(-s,-\ell)$ and $(s,-\ell)$. In the (r,θ) system the vertices would be located at (r_1,θ_1), (r_2,θ_2), (r_3,θ_3) and (r_4,θ_4) where

$$r_1 = [(s - x)^2 + (\ell - y)^2]^{1/2}, \quad r_2 = [(s + x)^2 + (\ell - y)^2]^{1/2}$$

$$r_3 = [(s + x)^2 + (\ell + y)^2]^{1/2} \text{ and } r_4 = [(s - x)^2 + (\ell - y)^2]^{1/2}.$$

The corresponding angles are defined by

$$\cot\theta_1 = \frac{s - x}{\ell - y}, \quad \cot\theta_2 = \frac{-s - x}{\ell - y}, \quad \cot\theta_3 = \frac{s + x}{\ell + y} \text{ and } \cot\theta_4 = \frac{s - x}{-\ell - y}$$

Also we note that

$$r_o(\theta) = \begin{cases} \dfrac{\ell - y}{\sin\theta} & \text{for } \theta_1 \text{ to } \theta_2 \\ -\dfrac{s + x}{\cos\theta} & \text{for } \theta_2 \text{ to } \theta_3 \\ -\dfrac{\ell + y}{\sin\theta} & \text{for } \theta_3 \text{ to } \theta_4 \\ \dfrac{s - x}{\cos\theta} & \text{for } \theta_4 \text{ to } \theta_1 \end{cases} \qquad (59)$$

Thus (51) for the rectangular loop takes the form

$$f(\lambda) = \frac{1}{A\lambda}\left\{\int_{\theta_1}^{\theta_2} J_1\left[\lambda\,\frac{(\ell - y)}{\sin\theta}\right]\frac{\ell - y}{\sin\theta}\,d\theta + \int_{\theta_2}^{\theta_3} J_1\left[-\lambda\,\frac{s + x}{\cos\theta}\right]\left[\frac{-(s + x)}{\cos\theta}\right]d\theta\right.$$
$$\left. + \int_{\theta_3}^{\theta_4} J_1\left[-\lambda\,\frac{(\ell + y)}{\sin\theta}\right]\left[\frac{-(\ell + y)}{\sin\theta}\right]d\theta + \int_{\theta_4}^{\theta_1} J_1\left[\lambda\,\frac{s - x}{\cos\theta}\right]\left[\frac{s - x}{\cos\theta}\right]d\theta\right\} \tag{60}$$

The integrals in (60) can be evaluated either by direct numerical integrations on θ or by the following series approach.

These integrals are of two types that can be defined as

$$\int_0^{\theta_o} \frac{1}{\cos\theta}\,J_1\left(\frac{\beta}{\cos\theta}\right)d\theta = C(\beta,\theta_o) \tag{61}$$

and

$$\int_{\theta_o}^{\pi/2} \frac{1}{\sin\theta}\,J_1\left(\frac{\beta}{\sin\theta}\right)d\theta = S(\beta,\theta_o) \tag{62}$$

These can be handled by using the series formulas for the Bessel function, i.e.,

$$J_1(\alpha) = \sum_{m=0}^{\infty} B_m \alpha^{2m+1} \tag{63}$$

where

$$B_m = (-1)^m \frac{1}{m!(m + 1)!\,2^{2m+1}}$$

Then clearly

$$C(\beta,\theta_o) = \sum_{m=0}^{\infty} B_m \beta^{2m+1}\, C_m(\theta_o) \tag{64}$$

and

$$S(\beta,\theta_o) = \sum_{m=0}^{\infty} B_m \beta^{2m+1}\, S_m(\theta_o) \tag{65}$$

where

$$C_m(\theta_o) = \int_0^{\theta_o} \frac{1}{(\cos\theta)^{2m+2}}\,d\theta \tag{66}$$

and

$$S_m(\theta_o) = \int_{\theta_o}^{\pi/2} \frac{1}{(\sin\theta)^{2m+2}}\,d\theta \tag{67}$$

These are integrals of a standard type and we may write

$$C_o(\theta_o) = \tan \theta_o \tag{68}$$

$$C_1(\theta_o) = \tan \theta_o + \frac{\tan^3 \theta_o}{3} \tag{69}$$

$$C_2(\theta_o) = \frac{\sin \theta_o}{5 \cos^5 \theta_o} + \frac{4}{15} \frac{\sin \theta_o}{\cos^3 \theta_o} + \frac{8}{15} \tan \theta_o \tag{70}$$

For higher order values we have the recurrence formula

$$C_m(\theta_o) = \frac{\sin \theta_o}{(2m + 1)\cos^{2m+1} \theta_o} + \frac{2m}{2m + 1} C_{m-1}(\theta_o) \tag{71}$$

Similarly

$$S_o(\theta_o) = \cot \theta_o \tag{72}$$

$$S_1(\theta_o) = \cot \theta_o + \frac{\cot^3 \theta_o}{3} \tag{73}$$

$$S_2(\theta_o) = \frac{\cos \theta_o}{5 \sin^5 \theta_o} + \frac{4}{15} \frac{\cos \theta_o}{\sin^3 \theta_o} + \frac{8}{15} \cot \theta_o \tag{74}$$

and, for higher values,

$$S_m(\theta_o) = \frac{\cos \theta_o}{(2m + 1)\sin^{2m+1} \theta_o} + \frac{2m}{2m + 1} S_{m-1}(\theta_o) \tag{75}$$

In the evaluation of $f_x(\lambda)$ and $f_y(\lambda)$ for the rectangular loop, (57) and (58) take the following forms:

$$f_x(\lambda) = \frac{1}{\lambda A} \int_{-\ell}^{\ell} [J_o(\lambda \hat{\rho})\big|_{x'=s} - J_o(\lambda \hat{\rho})\big|_{x'=-s}]dy' \ . \tag{76}$$

and

$$f_y(\lambda) = \frac{1}{\lambda A} \int_{-s}^{s} [J_o(\lambda \hat{\rho})\big|_{y'=\ell} - J_o(\lambda \hat{\rho})\big|_{y'=-\ell}]dy' \tag{77}$$

In general the evaluation of (76) and (77) requires numerical integration.

NUMERICAL RESULTS

In this section we present numerical results for the fields of both circular and rectangular buried loops. The half space is taken to be homogeneous ($\sigma_1 = \sigma_2$ and $\varepsilon_1 = \varepsilon_2$), and the frequency is sufficiently low that displacement currents

are negligible ($\sigma_1 >> \omega\varepsilon_1$). The following dimensionless parameters are utilized in presenting the numerical results:

$$Z = z/h, \quad H = h(\omega\mu_o\sigma_1)^{1/2}, \quad D = (x^2 + y^2)^{1/2}/h, \quad \text{and} \quad \phi = \text{Arc tan } (y/x) . \tag{78}$$

Although computer programs were written to evaluate the fields at any arbitrary location above the half-space, all results are presented for the observer at the surface ($Z = 0$).

The results for the circular loop were obtained by numerical integration of (32) and (33). In Figures 3 and 4, we illustrate the vertical and horizontal magnetic fields for various loop sizes for the static case ($H = 0$). As expected, the response is stretched out as a/h is increased. Of course, the results are independent of ϕ for circular loops.

The results for rectangular loops were obtained by numerical integration of (43) and (44). The results for the horizontal fields are given terms of radial and azimuthal components P_ρ and P_ϕ:

$$P_\rho = P_x \cos\phi + P_y \sin\phi \tag{79}$$

and

$$P_\phi = P_y \cos\phi - P_x \sin\phi \tag{80}$$

The normalized loop dimensions S and L are defined as

$$S = s/h \quad \text{and} \quad L = \ell/h . \tag{81}$$

In Figures 5 and 6, $|P_z|$ and $|P_\rho|$ are shown for various size rectangular loops for $S/L = 2$ and $\phi = 0°$. Due to symmetry, P_ϕ is zero for $\phi = 0°$. Note that for $S = 0$ the results reduce to those of the circular loop for $a/h = 0$. This simply confirms the result that a small loop looks like a magnetic dipole regardless of the shape.

In Figures 7 and 8, the ϕ dependence of all three components is shown for two different size loops. Because of symmetry, P_ϕ is zero at $\phi = 0°$ and $90°$, and only the range from $\phi = 0°$ to $90°$ need be shown. Note that the

larger loop (S = 2) in Figure 8 produces a greater ϕ variation and a larger P_ϕ.

In Figures 9-12, the effect of earth conductivity (H = 2 and H = 5) is shown for the same loop parameters as in Figures 5 and 6. The primary effect of increasing H is to attenuate the field and to fill in the nulls in P_z.

CONCLUDING REMARKS

Expressions have been derived for the magnetic field in air produced by a buried horizontal loop of arbitrary shape. In general the functions which characterize the particular loop shape, $f(\lambda)$, $f_x(\lambda)$, and $f_y(\lambda)$, require a single numerical integration as indicated by (49), (57), and (58). For the particular case of a rectangular source loop, (49), (57), and (58) reduce to the integrals given by (59), (76), and (77). These forms have been programmed to produce the numerical results given in Figures 5-12. For the special case of a circular loop, the results simplify in terms of Bessels functions, but a numerical integration over the wavenumber λ is still required as indicated by (32) and (33).

The numerical results in Figures 3-6 indicate that small rectangular and circular loops produce similar surface fields, but that differences appear as the loop size is increased. In particular the ϕ symmetry, that exists for circular loops is lost when the loop is rectangular. Also, an azimuthal component of magnetic field is produced by the rectangular loop as shown in Figs. 7 and 8. This field component could present a problem in source location.

An important limitation of the present formulation is that the current in the loop is assumed to be uniform. This is justified on the basis that the loop wire conductor is covered by insulation and that the circumference of the loop is extremely small compared with the wavelength in the insulation. At radio frequencies and higher, this assumption is clearly violated and another approach, such as the integral equation technique of Chang (1973) would have to be implemented

A worthwhile further extension of the present analysis is to allow for tilts of the source loop relative to the air/earth interface. The formulation for this case is complicated by the vertical components of the source currents but no fundamental difficulty should be encountered. Of course, the implementation of the numerical task would not be trivial. This is certainly a valid subject for further effort.

Acknowledgements

We would like to thank Robert McDonald and Jeri L. Bacon for their help in preparing the illustrations and manuscript.

APPENDIX B

The Three-Layer Case

With reference to Fig. 13, it not difficult to show that the function $T(\lambda)$ analogous to (30) is given by

$$T(\lambda) = D^{-1}\left(\frac{2u_2}{u_2 + u_3}\right)\left(\frac{2u_1}{u_1 + u_2}\right)\left(\frac{2\lambda}{u_1 + \lambda}\right) \exp[-u_3(h - c) - u_2(c - b) - u_1 b] \quad (1)$$

where

$$D = 1 - \left(\frac{u_2 - u_3}{u_2 + u_3}\right)\left(\frac{u_2 - u_1}{u_2 + u_1}\right) \exp[-2u_2(c - b)]$$

$$- \left(\frac{u_1 - \lambda}{u_1 + \lambda}\right)\left(\frac{u_1 - u_2}{u_1 + u_2}\right) \exp[-2u_1 b] \quad (2)$$

$$- \left(\frac{u_1 - \lambda}{u_1 + \lambda}\right)\left(\frac{u_2 - u_3}{u_2 + u_3}\right) \exp[-2u_1 b - 2u_2(c - b)]$$

where $u_m = (\lambda^2 + \gamma_m^2)^{1/2}$, $\gamma_m^2 = i\sigma_m \mu_o \omega$ for $m = 1,2,3$. Here $\mu_m = \mu_o$ and all displacement currents are ignored.

The three quantities in large parentheses on the right-hand side of (1) are the transmission coefficients for the interfaces at $z = -c$, $-b$ and 0 respectively. The total complex phase is given by the exponential term in (1). The total effect of the internal reflections are included in the expression for D given by (2).

The expression for D was given incorrectly in the report by Wait and Spies [1971b]. I am grateful to Dr. Thurlow W.H. Caffey, who pointed this out.

REFERENCES

CHANG, D.C., (1973), Characteristics of a horizontal loop antenna over a multi-layered, dissipative half-space, *IEEE Trans.*, AP-21, No. 6, 871-874.

LARGE, D.G., BALL, L., and FARSTAD, A.J., (1973), Radio transmission to and from underground coal mines - theory and experiment, *IEEE Trans.*, COM-21, No. 3, 194-202.

WAIT, J.R., and SPIES, K.P. (1971a), Electromagnetic fields of a small loop buried in a stratified earth, *IEEE Trans.*, AP-19, No. 5, 717-718.

WAIT, J.R., and SPIES, K.P., (1971b), Evaluation of the surface EM fields for a buried magnetic dipole, *AFCRL Rep. 52*, (available from N.T.I.S., Springfield, Va. 22151).

WAIT, J.R., (1971), Electromagnetic induction technique for locating a buried source, *IEEE Trans.*, GE-9, No. 2, 95-98.

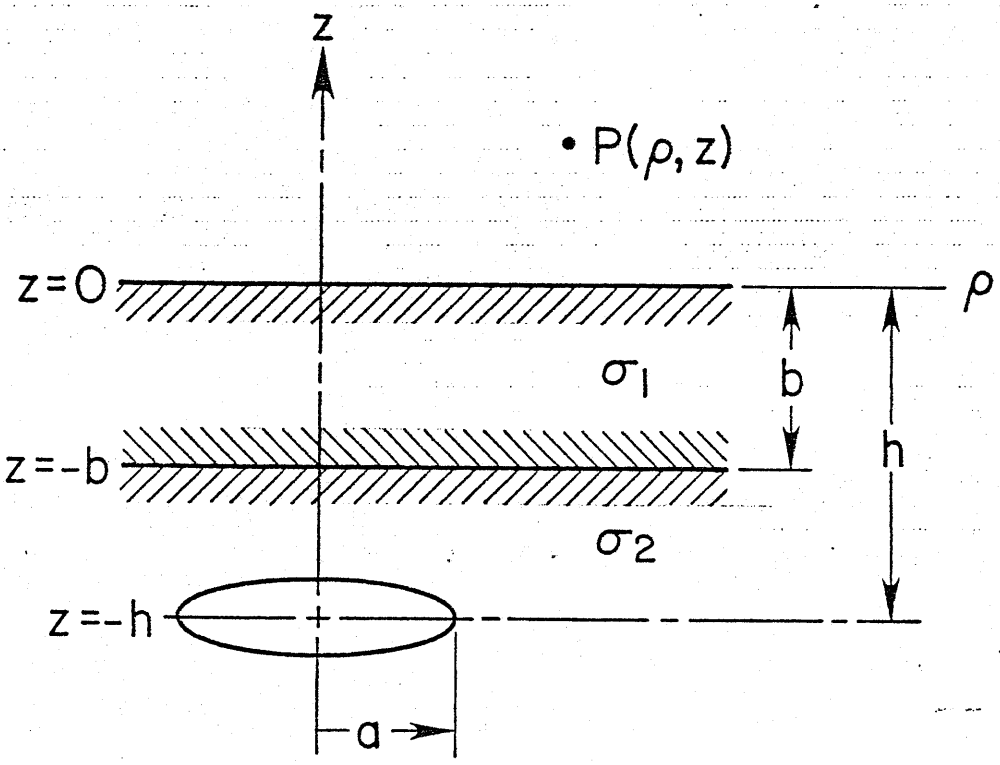

Circular loop of radius a buried in a two layer earth.

Fig. 1

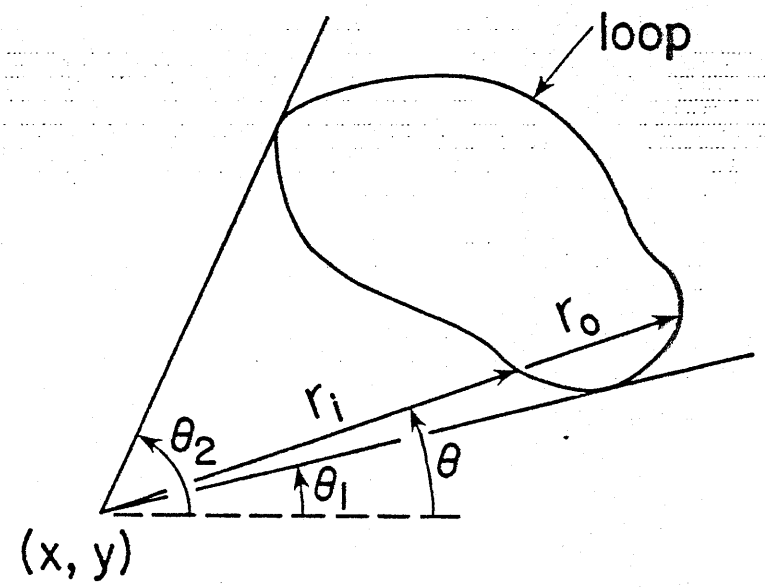

Geometry for a loop of arbitrary shape.

Fig. 2

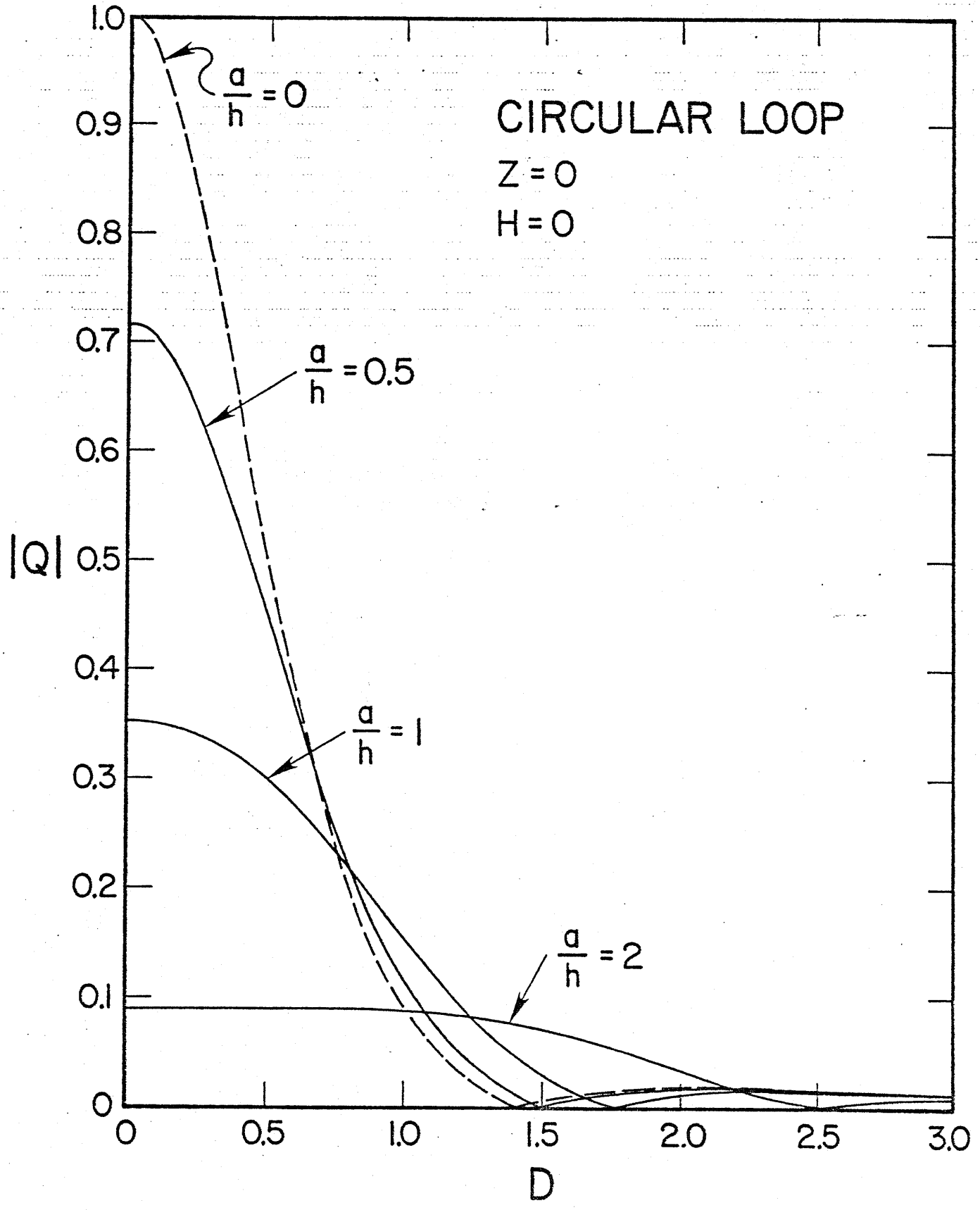

Vertical component of normalized magnetic field for circular loops of various sizes.

Fig. 3

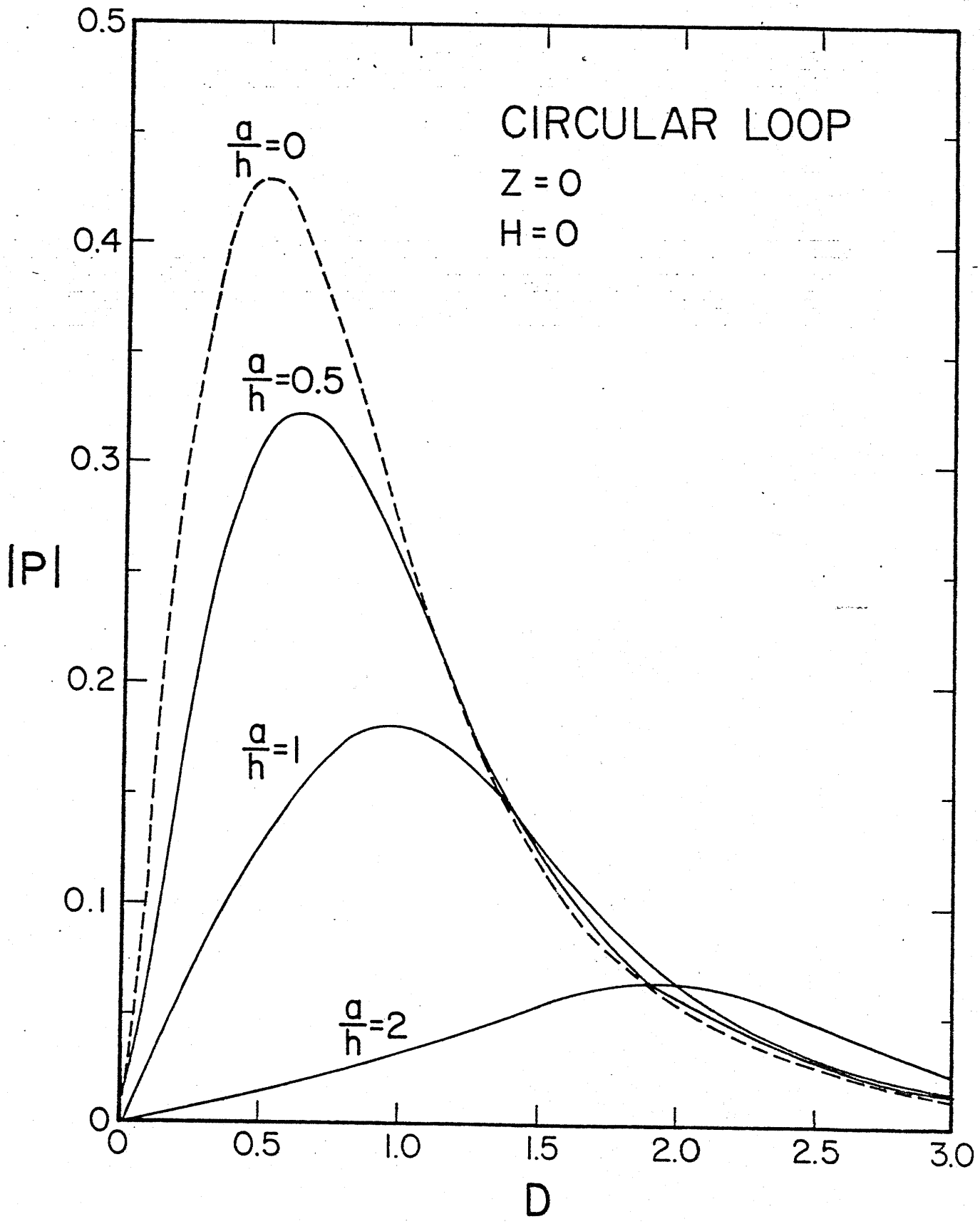

Horizontal component of normalized magnetic field for circular loops of various sizes. Fig. 4

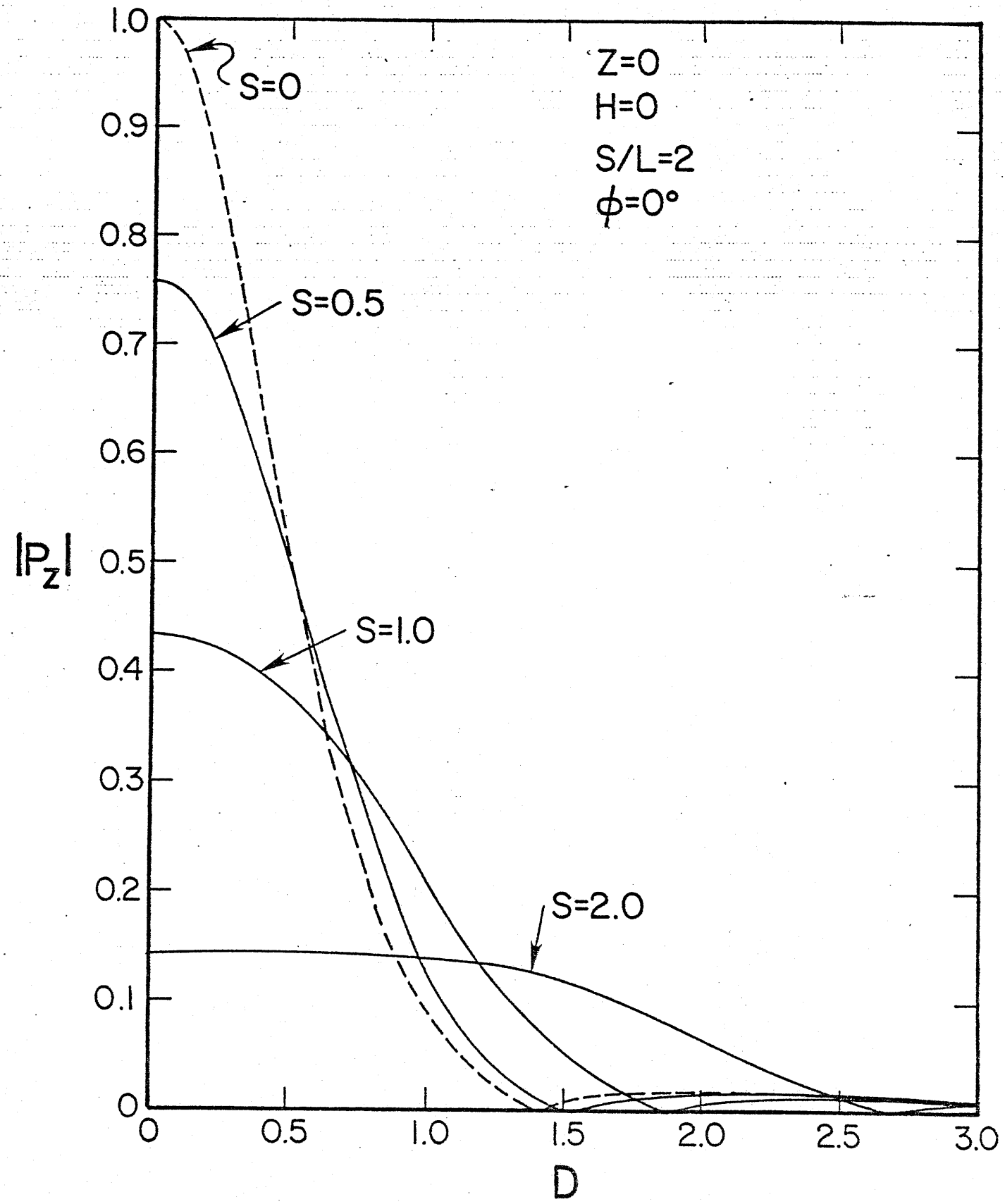

Vertical component of normalized magnetic field for rectangular loops of various sizes. Fig. 5

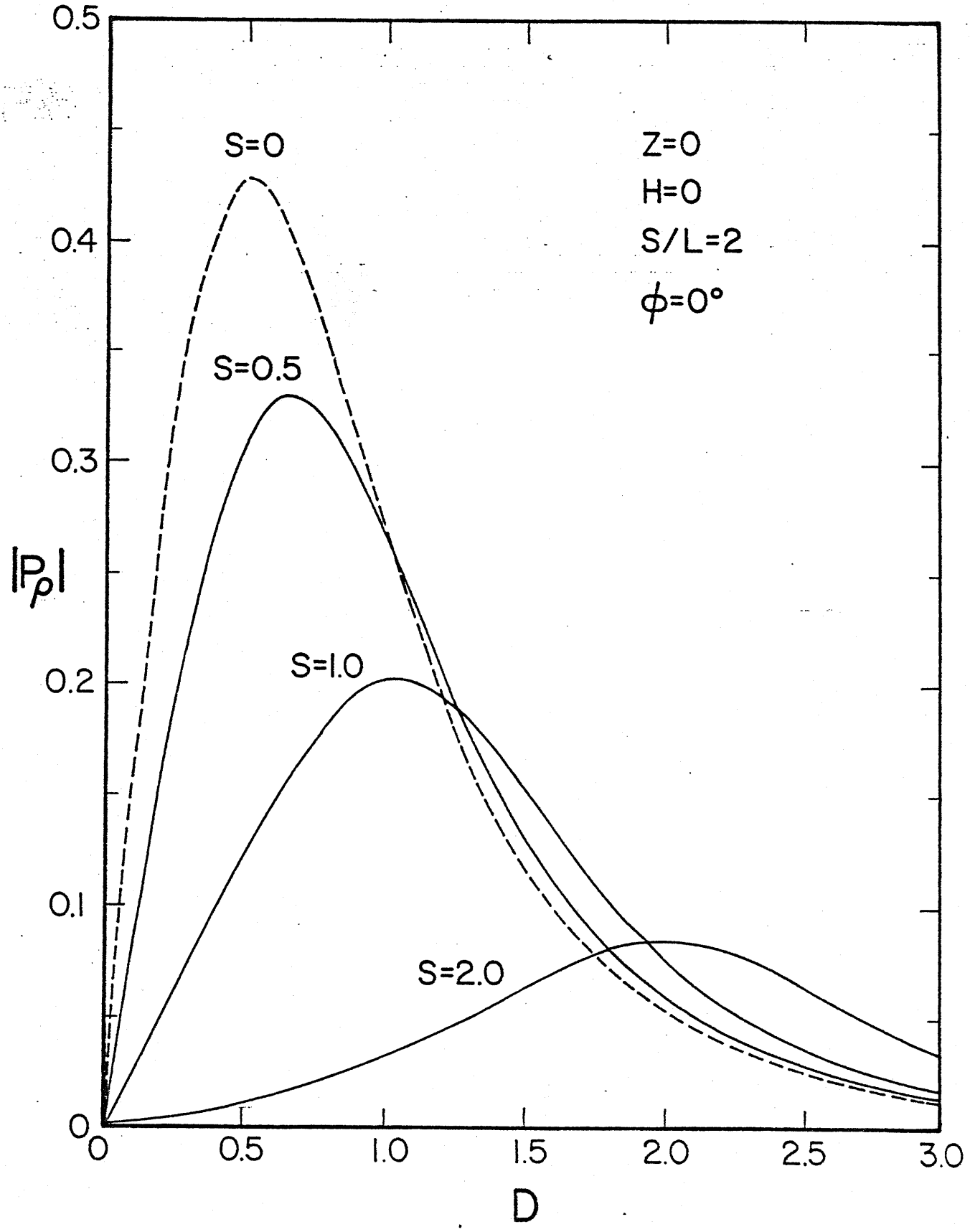

Radial component of normalized magnetic field for rectangular loop of various sizes. Fig. 6

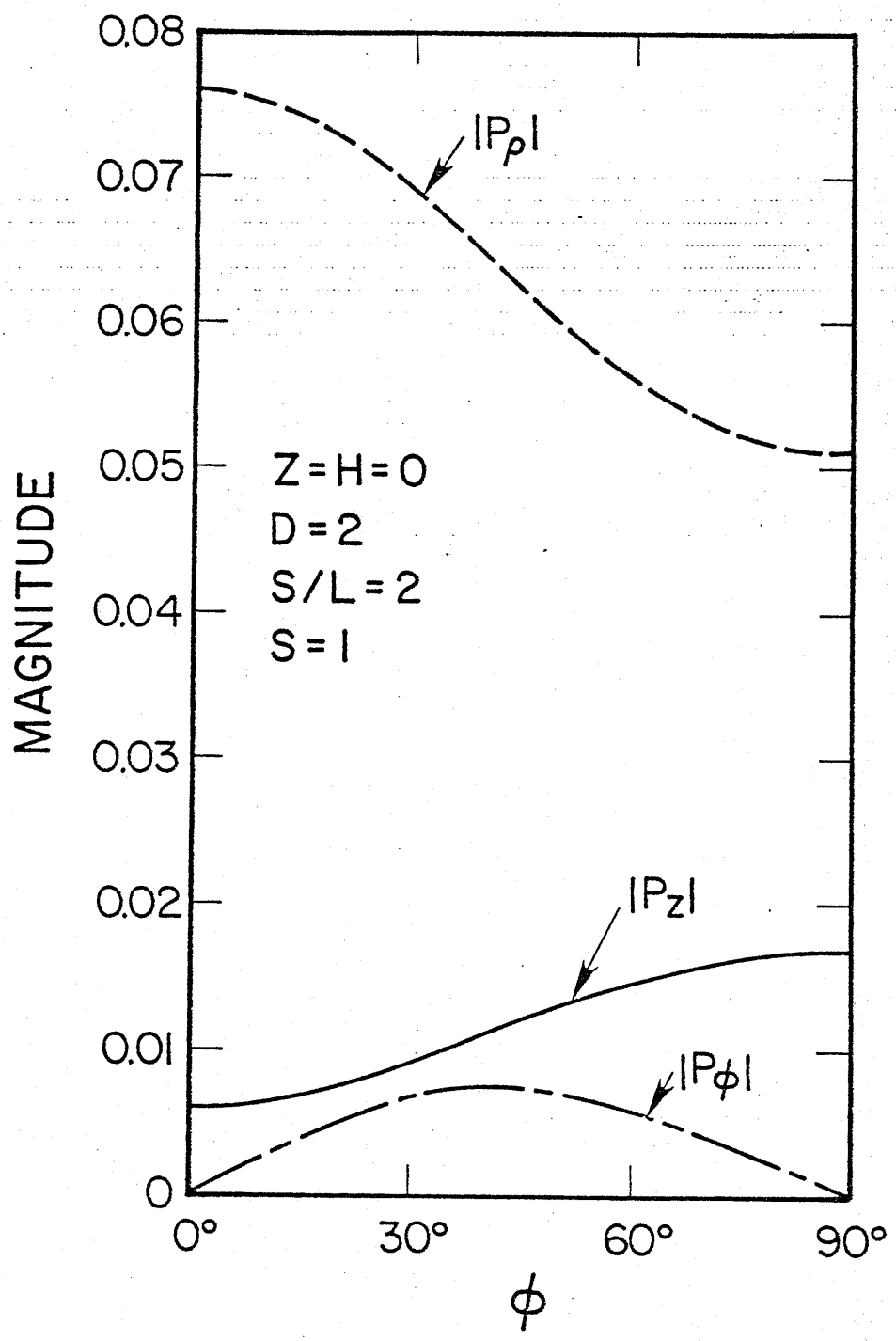

The azimuthal dependence of the three components of magnetic field for a rectangular loop. Fig. 7

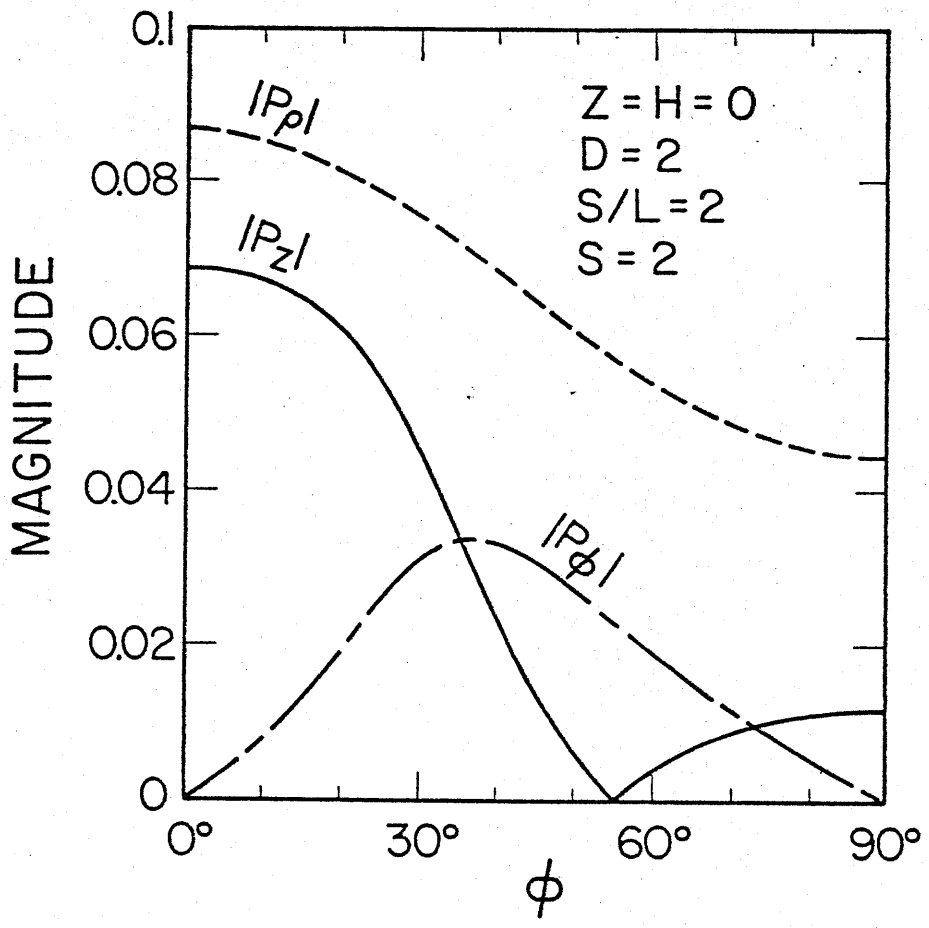

Fig. 8 The azimuthal dependence of the three components of magnetic field for a larger rectangular loop (S=2)

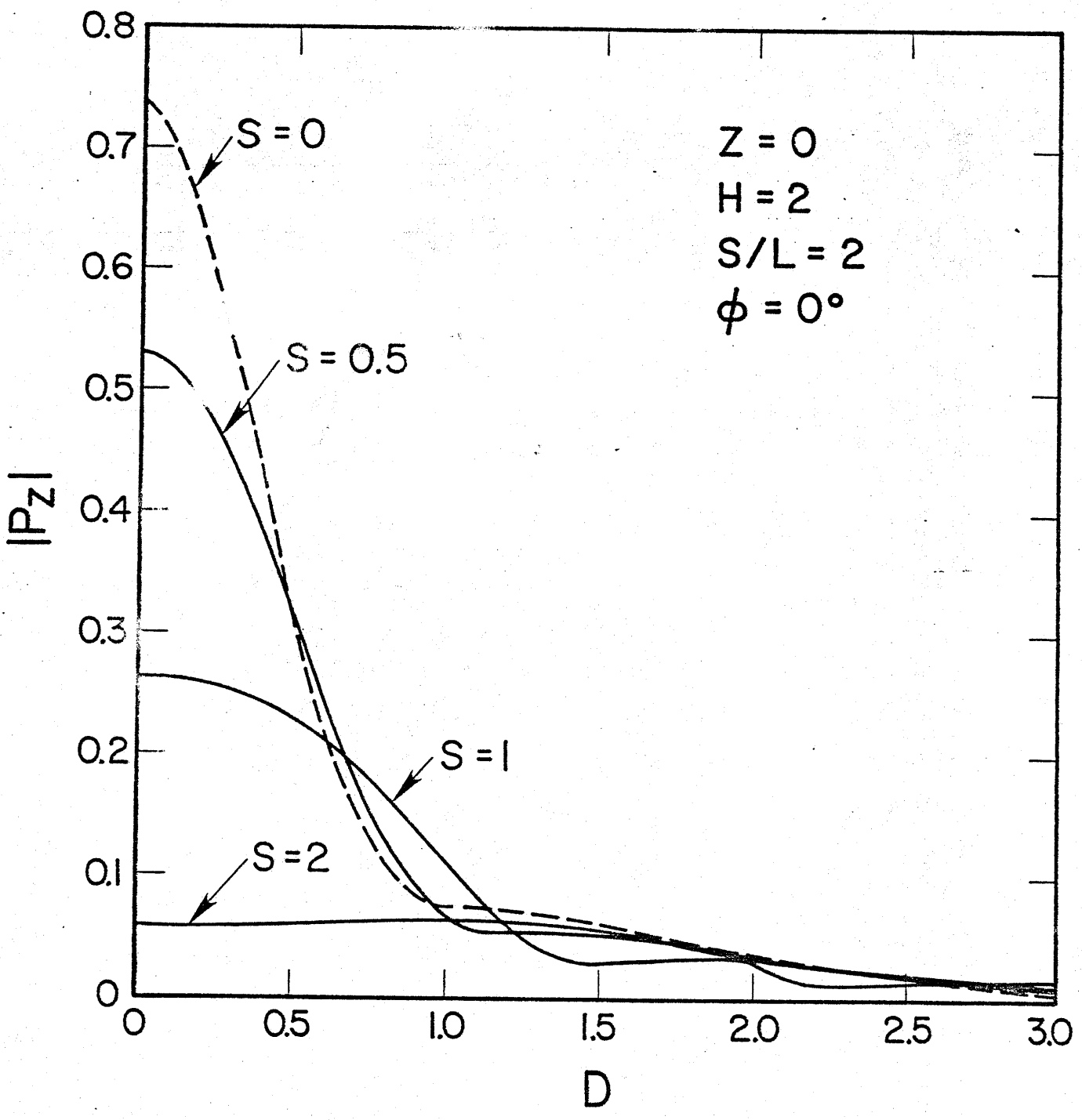

Vertical component of normalized magnetic field for a rectangular loop for H = 2. Fig. 9